UNIVERSITY OF SÃO PAULO
ESCOLA POLITÉCNICA

LUIZ CARLOS GOMES FILHO

Well production optimization under the scale effect and CO_2-WAG injection in Brazilian pre-salt

São Paulo
2024

LUIZ CARLOS GOMES FILHO

Well production optimization under the scale effect and CO_2-WAG injection in Brazilian pre-salt

Revised Version

Dissertation presented to the Graduate Program in Oceanic and Naval Engineering at the Escola Politécnica, University of São Paulo, to obtain the degree of Master of Science.

Concentration area: Naval and Oceanic Engineering

Advisor: Prof. Dr. Marcio Augusto Sampaio Pinto

São Paulo
2024

Catalogação-na-publicação

Gomes Filho, Luiz Carlos
Well production optimization under the scale effect and CO_2-WAG injection in Brazilian pre-salt / L. C. Gomes Filho -- São Paulo, 2024.
107 p.

Dissertação (Mestrado) - Escola Politécnica da Universidade de São Paulo. Departamento de Engenharia Naval e Oceânica.

1.Scale 2.Formation Damage 3.CO2-WAG 4.Reactive Flow 5.Numerical Simulation I.Universidade de São Paulo. Escola Politécnica. Departamento de Engenharia Naval e Oceânica II.t.

GOMES FILHO, L. C. **Well production optimization under the scale effect and CO_2-WAG injection in Brazilian pre-salt**. 2024. 107 p. Dissertation (Master of Science) – Escola Politécnica, University of São Paulo, São Paulo, 2024.

Aprovado em:

Banca examinadora

Prof. Dr. _____

Instituição: _____

Julgamento:_____

Prof. Dr. _____

Instituição: _____

Julgamento:_____

Prof. Dr. _____

Instituição: _____

Julgamento:_____

Dedicated to Luiz Carlos Gomes, in memory.

ACKNOWLEDGEMENTS

The author thanks the University of São Paulo, in particular the departments of Naval and Ocean Engineering and Mining and Petroleum Engineering, and Petrobras for supporting this work. He also appreciates the LASG team, especially to researcher Leonardo Fonseca Reginato and Petrobras professionals Lucas Duarte Beggiato, Fernando Lermen Pinheiro, Diego Cavalcanti Perrelli, Roni Fabio Dalla Costa, Luciano Endres, Leonardo Kubota, Renato Poli, Daniel Hallack, Aline Machado de Azevedo Novaes, Emerson Luiz Maneira, Manoel de Sá Jardim Neto, Patrícia Braga Gusmão and other colleagues for their patience and availability for clarification. CEPETRO team is tanked for the development and public availability of the UNISIM-III model.

Special thanks to Professor Dr. Márcio Augusto Sampaio Pinto for his guidance in this work, and to Professors Dr. Jean Vicente Ferrari and Dr. Marcos Allyson Felipe Rodrigues for their valuable suggestions for improvement. Also, thanks to Hydra Rodrigues for the clarifications and information provided.

Finally, I would like to thank my wife Simone and my children Isabel, Thomas, Catarina, and João Pedro for their tremendous patience and support throughout the years of developing this work.

"One who is not prepared for adversity is always subject to be defeated by it."

(Epictetus)

RESUMO

Este trabalho ressalta a importância de considerar o efeito da incrustação na simulação numérica e no gerenciamento do reservatório. A incrustação pode causar problemas operacionais e reduzir a produtividade dos poços. Ao considerar o efeito da incrustação na previsão, é possível evitar curvas de produção superestimadas e garantir uma estimativa mais precisa do comportamento produtivo dos poços ao longo do tempo, permitindo um gerenciamento otimizado da campanha de tratamentos e das operações de troca de fluidos WAG-CO_2 na jazida. Este estudo apresenta uma metodologia inovadora que permite o cálculo integrado da incrustação que ocorre no meio poroso de reservatórios de grandes dimensões e o que ocorre próximo aos canhoneios dos poços produtores, cujos efeitos são de difícil captura por simulações de fluxo de transporte reativo nos modelos de grande escala. Com a metodologia proposta, foi possível avaliar os efeitos da incrustação na redução da produtividade dos poços produtores, bem como no meio poroso, permitindo o gerenciamento otimizado da campanha de tratamento e das operações de troca de fluidos WAG-CO_2 na jazida. Ao longo do estudo, foram obtidos resultados quantitativos significativos, demonstrando a eficácia da metodologia proposta na otimização das injeções de WAG-CO_2 e dos tratamentos de incrustação nos canhoneios de poços, utilizando um modelo de reservatório baseado no Pré-Sal brasileiro. A pesquisa consistiu em duas fases de desenvolvimento metodológico. A primeira fase envolveu a criação de uma proxy simplificada do simulador de equilíbrio químico para calcular a massa precipitável de incrustação. Nessa fase, o processo de otimização foi realizado em duas etapas: otimização de WAG-CO_2 e otimização subsequente dos tratamentos. A metodologia foi aplicada em um recorte do modelo de fluxo completo (UNISIM-III), resultando em melhorias no Valor Presente Líquido (VPL) em comparação com outras soluções, com destaque para a importância do uso do método WAG-CO_2 e da otimização do gerenciamento dos tratamentos de limpeza e inibição de incrustação. O estudo também comparou os tratamentos realizados remotamente ou através de sondas. Os resultados da primeira fase indicam que há sempre vantagem econômica em realizar tratamentos remotos em vez daqueles realizados por sondas. Outra conclusão importante foi que o ponto ótimo para os tratamentos nem sempre coincidiu com a realização de tratamentos preventivos. Na segunda fase de desenvolvimento metodológico, a proxy para o cálculo da massa precipitável nos canhoneios de poços foi refinada por meio do desenvolvimento estatístico de uma expressão analítica que permitiu o cálculo correlacionado da massa precipitável com a composição da água produzida, durante o tempo de simulação de fluxo. Nessa fase, o processo de otimização das injeções de WAG-CO_2 e dos tratamentos foi conduzido em etapa única. Essa metodologia aprimorada foi aplicada ao modelo completo do UNISIM-III, composto por seis poços produtores e sete injetores de WAG-CO_2 interconectados a uma Unidade Estacionária de Produção (UEP). A solução ótima (OS) obteve um aumento significativo no VPL em relação aos casos de comparação, com destaque para o cenário em que os tratamentos não são realizados, onde a OS resultou em um ganho de 2,459 bilhões de dólares no VPL. Em conclusão, o estudo desenvolvido forneceu *insights* valiosos para as decisões de gestão integrada das injeções de WAG-CO_2 e dos tratamentos de incrustação nos canhoneios de poços. Os resultados destacam a importância de considerar os efeitos de incrustação e implementar estratégias otimizadas para maximizar o valor econômico em reservatórios que produzem sob risco de incrustação.

Palavras-chave: incrustação, dano à formação, WAG-CO_2, fluxo reativo, simulação numérica.

ABSTRACT

This work highlights the importance of considering the effect of scale in numerical simulation and reservoir management. Scale deposition can cause operational issues and reduce well productivity. By accounting for scale effects in the prediction, it is possible to avoid overestimated production curves and ensure a more accurate estimation of well productivity over time. This enables optimized management of treatment campaigns and WAG-CO_2 fluid exchange operations in the reservoir. This study presents an innovative methodology that allows for the integrated calculation of scale occurring in the porous medium of large-scale reservoirs and near the perforations of producer wells, the latter of which is difficultly captured by flow reactive simulations transport models (FSRT) in large-scale models. With the proposed methodology, it was possible to assess the effects of scale on the reduction of well productivity, as well as on the porous medium, enabling optimized management of the treatment campaign and CO_2-WAG fluid exchange operations in the field. Throughout the study, significant quantitative results were obtained, demonstrating the effectiveness of the proposed methodology in optimizing CO_2-WAG injections and scale treatments in well perforations, using a reservoir model based on the Brazilian Pre-Salt. The research consisted of two phases of methodological development. The first phase involved the creation of a simplified proxy for the chemical equilibrium simulator to calculate the precipitable mass of scale. In this phase, the optimization process was conducted in two stages: CO_2-WAG optimization and subsequent treatment optimization. The methodology was applied to a cutout of complete flow model (UNISIM-III), resulting in improvements in Net Present Value (NPV) compared to other solutions, highlighting the importance of using the CO_2-WAG method and optimizing the management of scale cleaning and inhibition treatments. The study also compared treatments performed remotely or by rigs. The results of the first phase indicate that there is always an advantage in performing remote treatments rather than those performed through rigs. Another important conclusion was that the optimal point for treatment did not always coincide with the implementation of preventive treatments. In the second phase of methodological development, the proxy for calculating the precipitable mass in the well perforations was refined through the statistical development of an analytical expression that allowed for the correlated calculation of the precipitable mass with the composition of the produced water, during flow simulation time. In this phase, the optimization process for CO_2-WAG injections and treatments was conducted in a single step. This enhanced methodology was applied to the full UNISIM-III model, consisting of six producing wells and seven CO_2-WAG injectors interconnected to a Stationary Production Unit (SPU). The optimal solution (OS) achieved a significant increase in NPV in relation to the comparison cases, with emphasis on the scenario where no treatments are performed, where the OS resulted in a gain of 2.459 billion dollars in NPV. In conclusion, the developed study provided valuable insights for integrated management decisions regarding CO_2-WAG injections and scale treatments in well perforations. The results highlight the importance of considering the effects of scale and implementing optimized strategies to maximize economic value in reservoirs that produce under the risk of scale.

Keywords: scale, formation damage, CO_2-WAG, reactive flow, numerical simulation.

LIST OF FIGURES

LIST OF TABLES

LIST OF SYMBOLS

Symbols

B_o	Oil formation volume factor
BHP	Well bottom hole pressure, kPa
C_i	Production/injection cost of fluid stream i
CR	Corporate tax rate
C_{trat}	Current unit cost of treatments
$efic_{Trat}$	Cleaning treatment efficiency
f_{Inhib}^{p}	Inhibition factor calculated in simulation time p
EOS	Equation of state
h	Length of perforation well open to flow
J	Productivity index
N_{trat}	Number of treatments performed
K, K_d, K_r, K_{eq}	Absolute permeabilities respectively original, of the damage zone, of the removal zone and total equivalent of drainage zone, mD
Kro, Krw	Permeability relative to oil and water, respectively
M_{tot}, M, m	Cumulative precipitated mass (kg); precipitable mass rate per day (kg/day) and precipitable mass rate per day and volume ($kg/m^3/day$) respectively.
N	Total production days
NPV	Net present value
P	Oil price, USD
P_e	Static pressure of the drainage zone, kPa
P_m	Target to average reservoir pressure, kPa
P_w	Well bottom hole pressure, kPa
$q_{i,j}$	Production / injection rate of fluid i on day j in surface condition, m^3/d
q_{oil}, q_{water}	Oil and water production rate in surface condition, m^3/d
roy	Royalties rate
r_e, r_d, r_r, r_w	Radius of drainage, damaged region, removal region and inside the well, respectively., m
sr_{factor}^{p},	Productivity index reduction factor due to scale calculated in period p
$sr_{wct\ range}^{target}$,	Target for srp_{factor} below which a treatment is performed. It is specified for each class of water cut (wct) range.

st	Social taxes rates
sw	Water saturation
SWC	Size of the CO_2-WAG cycles, days
t	Daily discount rate
Wp^p, Wp^t	Respectively, the cumulative volumes of produced water up to a generic time p and up to the time t of the last treatment performed, with p >= t.
Φ,Φ_d	Original average porosity and average porosity of the damaged area
μ_o	Oil viscosity, cp
ρ	Scale density, kg/m^3

Indexes

i	index that identifies a specific stream belonging to {oil produced, water produced, gas produced, water injected, gas injected}
j	Index that identifies a specific production day
o	Initial simulation time
p	Generic simulation time
t	Identifies the last simulated time in which a treatment was performed
wct range	class of water cut (wct) range

Abbreviations

ANOVA	Analysis of Variance
CIM	Chemical Injection Mandrel
EOR	Enhanced Oil Recovery
FPSO	Floating Production Storage and Offloading
FSRT	Flow Simulation with Reactive Transport
GOR	Gas Oil Ratio
GS	General Solutions
IPR	Inflow Performance Relationship
MMP	Minimum Miscibility Pressure
NPV	Net Present Value
OS	The Optimal Solution
pH	Potential Hydrogen
SPU	Stationary Production Unit
SWC	Size of the CO_2-WAG cycles, in days
TPR	Tubing Performance Relation

USD	United States Dollar
WAG	Water Alternating Gas
WCT	Water Cut

SUMMARY

1. INTRODUCTION

In the current scenario of variability in oil prices (Figure 1) and great uncertainties as to the future market for this product, oil and gas projects may have tighter profit margins than those originally forecasted. Production losses and unforeseen cost increases pose a major threat to project economics.

Figure 1– Price history of oil since May 1987. Europe Brent Spot Price.

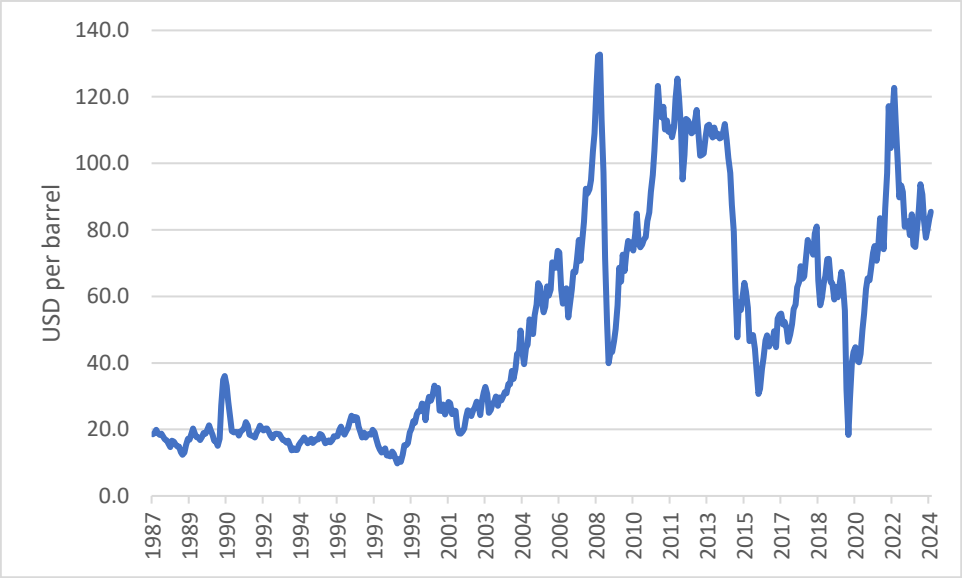

Source: EIA, 2024.

In this context, robustness in forecasting production curves and projecting operating costs is necessary. Therefore, it is essential to be proactively aware of the occurrence of events that will possibly lead to a decrease in productivity of producers, injectivity of injectors, or an increase in operating and maintenance costs, either through your prior knowledge or correct diagnosis of their root causes, to prevent and mitigate their occurrence. Of the events that can lead to large production losses, a very common one in the oil sector and difficult to predict is the occurrence of scale at points in the production flow.

According to Bader (2007), depositions can occur in virtually any part of the production system, from the reservoir, notably in the vicinity of producing and injector wells, well completion, passing through subsea flow lines, to surface equipment like valves, collectors, pumps, heat exchangers, separating vessels, and storage tanks. Yuan and Wood (2018) state that the deposition of materials harmful to the flow is caused by the incompatibility between fluids or variations in the thermodynamic conditions of the flow and can be of organic origin,

associated with the oil phase, as is the case with the depositions by asphaltenes and paraffins, or inorganic, associated with the aqueous phase. This last type of deposition is known in the oil and gas industry under the name scale.

The phenomenon of scale in oil production is associated with the aqueous phase and occurs mainly by mixing reactive waters with different characteristics and by varying thermodynamic conditions during the flow of fluids, either in the porous medium, or in the collection systems and production (Mackay et al., 2005). The precipitation of salts is quite undesirable, as it can cause severe restrictions to flow, causing damage to the reservoir, especially in the vicinity of producing and injector wells (Kang et al., 2020), with a consequent decrease in its rate of productivity, blocking production columns, lines, subsea and surface equipment. In the most severe cases, it can also cause the permanent loss of wells and the need for large expenses to clean subsea and surface equipment affected by deposition, with consequent loss of production and negative impacts on the profitability of the projects. In addition, the variation in the chemical composition and thermodynamic conditions of the waters can also cause the dissolution of rocks from the reservoir and the transport of the components to the production systems, where again they can find conditions for their precipitation to occur (Rodrigues et al., 2019). Figure 2 presents an example of scale caused by the deposition of Barium Sulfate and Strontium on sand control screens of a well.

Figure 2 – Barium and strontiun sulphate scale on sand screens.

Source: Rodrigues et al., 2007.

To maintain the profitability of projects subject to the occurrence of the phenomenon, it is necessary to prevent or removing the scale, which is done using inhibitors, cleaning of equipment and treatment of wells (Rodrigues et al., 2007). It happens that the treatment of wells for cleaning involves high costs, being common the need to use rings and support boats. For this reason, it is necessary to quantify the specific impacts of the scale on the loss of production from wells in order to economically evaluate the technical-economic viability of cleaning, since the decrease in production can also be caused by the effects of variation in relative permeability of fluids (Rosa et al., 2006). The total effect of the decrease in production can be observed by the drop in the productivity index (J) of wells, measured through pressure tests of Formation Evaluation area. However, as the decrease in J can be caused by the effects of variation in permeability relative to the oil (mobility effect), the correct diagnosis of the scale requires the joint analysis of several parameters, such as the ionic composition of the produced water, identification of pressure losses between the sensors along the flow and production history of the well and other wells in the field. If the scale diagnosis is not a simple task, its forecast is even more challenging, as it involves the need to predict formation saturations, water cuts, ionic compositions of fluids and pressure conditions of reservoir and lifting systems.

With the increase in computational efficiency, some approaches have emerged with the use of numeric flow simulation with reactive transport (FSRT) to evaluate the effect of exploitation under the reactivity of fluids and rocks in the reservoir, but none of them quantify the specific decrease in the productivity index caused by the localized scale in the perforation's well producers, in simulation models with large-scale.

1.1 Research objective.

1.1.1 General objective

This research proposes a workflow using FSRT coupled with scale and inhibition proxy models, which detail the region of the perforations, with the objective of predicting the occurrence of scale, quantifying the loss of production caused by it and determining the best campaign of operations for cleaning and inhibiting producers in carbonate reservoirs of the Brazilian pre-salt under the effect of incrustation and CO_2-WAG injection. Although the proposed workflow can be used for other types of salt deposits, this work addresses the scale caused by Calcite ($CaCO_3$), as it is the most observed deposition in the Brazilian pre-salt fields.

1.1.2 Specific objectives

The specific objectives are:

- Obtain the best configuration for CO_2-WAG fluid exchanges and optimal treatment campaign in a cutout of the UNISIM-III model, representative of the Brazilian Pre-Salt, containing one producer and two CO_2-WAG injectors, and subsequently in the full model with six producers and seven CO_2-WAG injectors;
- Comparison of treatments performed through well intervention versus those performed remotely by SPUs, the latter being less efficient but also lower in cost;
- Evaluation of treatments always performed preventively;
- Comparison of results obtained with those that do not use CO_2-WAG treatments and cases that do not consider scale effects.

1.2 Organization and content of the upcoming chapters

The content of the upcoming chapters is organized as follows. In the Literature Review chapter, various studies addressing the topic of reactive flow simulation and alternative analytical approaches to simulation are presented. The Methodology chapter presents the development of the proposed method, which enables the integrated calculation of scale occurring at the reservoir level and near the production well. The method was developed in two phases. In the first phase, a simplified proxy for calculating precipitable mass was created, and the optimization process was divided into two steps: CO_2-WAG optimization and treatment campaign optimization. The second phase involved refining the proxy of the chemical equilibrium simulator and optimizing both the CO_2-WAG variables and treatments in a single step. The Case Studies chapter showcases the application of the developed methodology through four cases. Cases 1 (CO_2-WAG optimization), 2 (rig treatments optimization), and 3 (remote treatments optimization) involve the application of the methodology developed in the first phase of development. Additionally, a cutout model of UNISIM-III with one producer well and two CO_2-WAG injectors was used. In Case 4 (CO_2-WAG and treatments optimization), the methodology from the second phase of development was applied to the complete UNISIM-III model, which includes six producer wells and seven CO_2-WAG injectors. In the Results and Discussions chapter, the main results of the case studies are presented, along with a comparison to the following benchmark cases:

- Cases that do not use the CO2-WAG method.
- Cases where treatments are always performed preventively.
- Cases where no treatments are performed.
- Cases that do not consider scale calculation in the perforations (overestimated results).

Finally, in the Conclusions chapter, the overall conclusions of the study are presented, along with recommendations for future work.

2. LITERATURE REVIEW

According to Mackay et al. (2005), scale in oilfields are inorganic crystalline deposits that form due to precipitation of solids from the brines present in the reservoir and in the production flow system. Precipitation of these solids occurs because of changes in the ionic composition, pH, pressure, and temperature of the brine. Mackay describes the three causes of scale formation. The first is the variation in pressure or temperature or pH of the brine that leads to a reduction in the solubility of the salt and which is most related to $CaCO_3$ depositions. The second cause is due to the mixture of incompatible brines, with different compositions, as is the case of the mixture that commonly occurs in oil reservoirs, where the connate water present in the formation and rich in ions such as calcium, barium and strontium meets injected sea water, with a high content of sulfate, leading mainly to the formation of scale by sulfates of barium, calcium, and strontium. The third cause is the evaporation of the brines causing oversaturation of the dissolved salts and resulting in their precipitation. In the latter case, NaCl depositions stand out. According to the authors, scale can be quite harmful to the oil and gas industry and some of its main consequences are:

a) severe flow restrictions throughout the production process;
b) reduction in the productivity index due to damage to the reservoir in the vicinity of the wells;
c) blocking of production columns, lines, subsea and surface equipment;
d) definitive loss of wells and drainage lines, in the most serious cases;
e) high maintenance costs for cleaning equipment affected by salt deposition;
f) high treatment costs and preventive well inhibition;
g) negative impacts on project profitability;
h) possible environmental and health impacts for operators caused by radioactive deposits such as radium salts.

Figure 3 shows the (a) picture of organic deposition, (b) inorganic deposition by barium sulfate in a duct and (c) separating vessel, with almost total obstruction of the area open to flow.

Figure 3 – Oil flow duct obstruction due to (a) paraffin and asphaltene, (b) barium sulfate scale and (c) scale in a production separator.

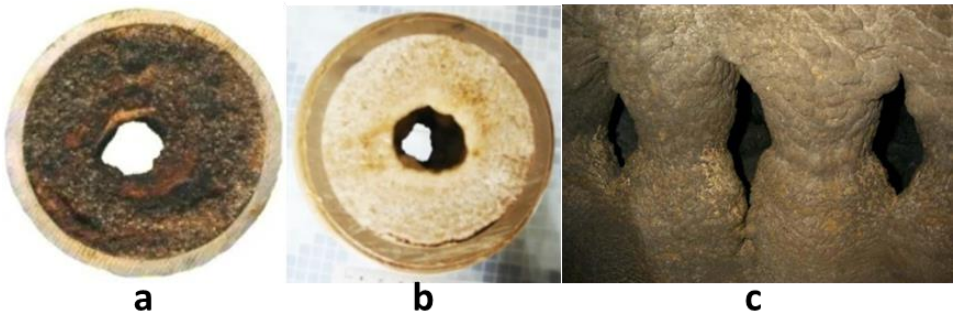

Sources: a – https://www.arab-oil-naturalgas.com/oilfield-paraffin-and-asphaltene/; b – www.engenhariae.com.br; c – https://www.spe.org/dl/docs/2008/Mackay.pdf.

Rodrigues et al. (2007) present the mechanism by which the scale alters the operating point given by the intersection of the pressure curves provided by the reservoir and required by the elevation systems (Figure 5a). The decrease in the flow of a producer under the effect of scale can be understood through the effects that scale provides to the interaction between the pressure curves provided by the reservoir, Inflow Performance Relationship (IPR), and the pressure curves required by the systems of elevation, Tubing Performance Relation (TPR), shifting the operating point given by the encounter between these two curves. In the reservoir, the occurrence of scale in the vicinity of the well causes a clockwise shift of the IPR curve, causing the operating point to change from Point A to B and the liquid flow rate to drop from Qa to Qb. In the well (usually in the production column and flow lines), scale causes flow restriction with a consequent increase in pressure loss. This effect translates into a generalized increase in the TPR curve, moving the operating point from A to B', and a drop in the flow rate to Qb'. The combined effects of scale on the lift and reservoir systems result in operating point C, causing an overall decrease in flow to Qc.

The dynamics of salt scale is related to the aqueous phase where, under certain thermodynamic conditions, there is supersaturation and deposition of the initially dissolved salts. Figure 5b shows the steps for the phenomenon to occur.

Bedrikovetsky et al. (2009) present an analytical model for predicting the scale caused by barium sulfate. The developed model is based on laboratory experiments, mass balance equations between the ions present in the solution and the deposited salt, together with the decrease in permeability explained by Darcy's law. In the article, the authors present a scheme of scale formation in the reservoir show in Figure 4. The diagram shows that the mixing zone between the formation and injected water corresponds to the most critical region for the occurrence of deposition in the reservoir, because of mixture of waters.

Figure 4 – Mechanism of barium sulfate scale in the reservoir caused by the mixture of injected seawater and formation water.

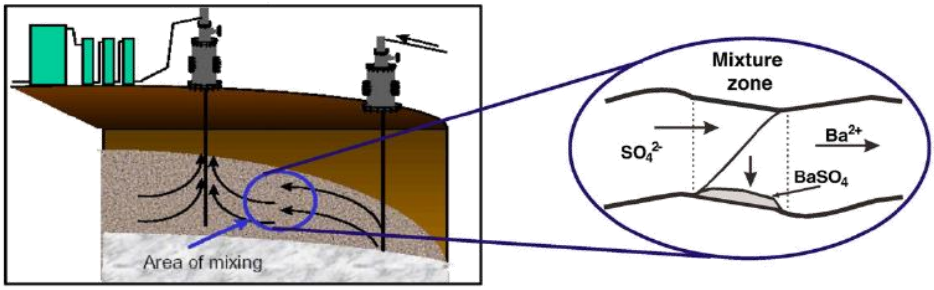

Source: Extracted from Bedrikovetsky et al. (2009).

According to Chauhan et al. (2015), as shown in Figure 5b, initially the salt in solution finds conditions of supersaturation due to variations in pressure, temperature, pH or even reactivity with rocks and other aqueous components. Nucleation then occurs, which consists of the appearance of the first crystals, which serve as an inducing seed for new deposition, with consequent growth of the crystals and adherence to the surfaces of the flow system. If the process continues, scale occurs. The inhibitors act precisely in the nucleation and crystal growth phases preventing the formation of nucleating particles and chemically adhering to their surfaces, preventing their growth and adherence to the pores of the reservoir and the walls of the production systems.

Figure 5 – Scale mechanism. (a): change in the balance point of production between TPR and IPR caused by the occurrence of scale. (b): phases of the scale formation process.

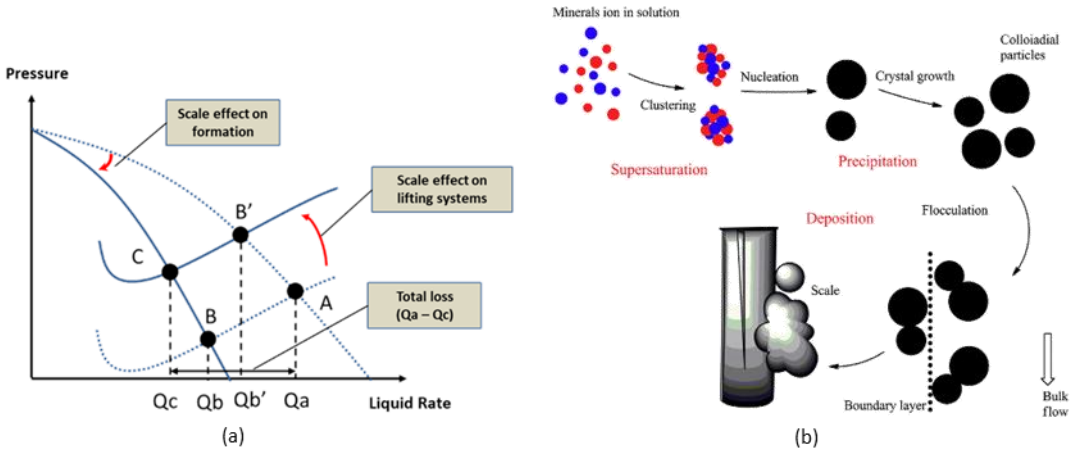

Sources: (a) adapted from Rodrigues et al. (2007), (b) phases of the scale formation process, Chauhan et al. (2015).

Novaes (2016) presents the most observed ions and reactions in carbonate reservoirs. The reactions are shown in Table 1.

Table 1 – Main reactions related to the scale in carbonate reservoirs.

Calcite	$CaCO_3 + H^+ \leftrightarrow Ca^{+2} + HCO_3^-$
Dolomite	$2CaCO_3 + Mg^{-2} \leftrightarrow Ca^{+2} + CaMg(CO_3)_2$
Celestite	$Sr^{+2} + SO_4^{-2} \leftrightarrow SrSO_4$
Barite	$Ba^{+2} + SO_4^{-2} \leftrightarrow BaSO_4$

Source: Novaes (2016).

Kamal et al. (2018) list, in Table 2, the common depositions in the oil industry associated with each type of reservoir (carbonates and sandstones), with their percentages of occurrence in mass.

Table 2 – Occurrence of the main types of incrustation by type of reservoir.

Carbonate		**Sandstones**	
Scale Type	**wt%**	**Scale Type**	**wt%**
Iron Sulfide	29.2	Calcium Carbonate	33.5
Iron Oxide	28.1	Iron Oxide	30.3
Silicon Oxide	10.4	Silicon Oxide	28.5
Iron Hydroxide	9	Iron Sulfide	1.7
Iron Carbonate	5.5	Iron Carbonate	2.5
Dolomite	4.6	Barium Sulfate	1.1
Calcium Carbonate	3.8	Magnesium Oxide	0.6
Calcium Sulfate	3.6	Aluminum Oxide	0.5
Chlorite	2.2	Strontium Oxide	0.5
Sodium Chlorite	1.4	Aluminum Silicate	0.4
Barium Sulfate	1.3	Chromium Oxide	0.2
Aluminum Silicate	0.9	Others	0.1
Molybdenum oxide	0.2		

Source: Kamala et al. (2018).

Depositions related to corrosion products from equipment account for the majority reported in Table 2. This result is mainly related to the souring effect in reservoirs that have significant levels of H_2S or that use water injection without desulfation and removal of O_2. In fields with low H_2S content and conditioned injected water, however, corrosion products are minimized, and depositions caused by calcium, barium, and strontium scale gain importance. Mainly during the flow process of fluids produced from the reservoir to the well, at the well-reservoir interface (perforations), but also in other parts such as the production column, elevation through the collection lines to the SPU, and primary oil processing. With a focus on scale formation by calcium carbonate in carbonate reservoirs.

2.1 CO_2-WAG and the occurrence of scale.

Oil production activity naturally involves the removal of mass from the reservoir, which, during production, reduces the pressure to which the fluids are subjected in the porous medium, with a consequent reduction in productive energy. To extend the levels of good productivity for longer, it is necessary to replenish the reservoir mass, which is usually done through injectors. Due to their availability in offshore scenarios, the fluids commonly used are treated seawater and, in some cases, also a part of the produced gas (secondary recovery methods). Another technique is the use of injectors capable of injecting water alternated with miscible gas. This

strategy is one of the Enhanced Oil Recovery (EOR) methods and aims to increase the reservoir's recovery factor by reducing the saturation of residual oil and increasing the efficiency of sweeping, when compared to the exclusive water or gas injection strategy. Another benefit of using CO_2-WAG is that it allows for more flexible production management through chosen changes that positively impact the behavior of producers, for example, enabling the control of water cut and gas-oil ratio of these wells. The CO_2-WAG strategy also allows for greater retention of CO_2 by the reservoir, due to the hysteresis effect, which is a positive aspect in managing this greenhouse gas (Rodrigues et al., 2019). Most offshore reservoirs recently discovered in the Brazilian pre-salt make use of the EOR technique with CO_2-WAG (Sampaio et al., 2020) due to the availability of carbon dioxide present in the produced gas.

2.2 Comparison between different fluid injection strategies

Figure 6 presents a comparison between the three most common fluid injection strategies for oil recovery. Picture (A) in the figure represents gas injection. It is observed that, compared to other strategies, the gas sweeps a small area of the reservoir, displacing the oil and quickly reaching the producing well, causing gas breakthrough in the producer well. This effect occurs due to the significantly greater mobility of gas compared to oil, as gas viscosity is significantly lower than that of oil. An advantage of the strategy is that the residual oil is relatively low compared to that left by the water in (B). In the exclusive water injection strategy (B), there is a greater spread of water than that observed with the exclusive gas injection, which occurs because the mobility of water is lower than that of gas. However, there is still a significant water finger in the direction of the producer, as the mobility of water is still reasonably greater than that of oil, causing it to cut the oil and reach the producer quickly. Furthermore, due to the high immiscibility of hydrocarbons with water, much of the residual oil is left behind in the swept region. The miscible CO_2-WAG strategy (C) aims to unite the advantages arising from strategies (A) and (B), avoiding their disadvantages. Injected water and gas tend to take different paths in the porous medium, causing a greater spread of the swept area compared to previous methods and delaying the breakthrough of the injected fluids in the producer well. Additionally, as gas injection is miscible and the typical vertical permeability of pre-salt reservoirs is very low, sometimes with non-reservoir barriers, the effect of gravitational segregation is greatly reduced in the miscible CO_2-WAG method, increasing volumetric sweep efficiency. It is also observed that there is a small amount of residual oil in the region where the gas passed, as in scenario (B). However, in strategy (C), unlike the previous ones, there is a

large area of contact between the gas and water in the forward interface fronts of these fluids. This means that a significant amount of carbon dioxide, normally present in the gas, will be in contact with the water, increasing the acidity of the fluids in this contact region by the formation of carbonic acid, which is reactive to carbonate rocks in the reservoir. The decrease in fluid pH causes the carbonate rocks to dissolve, saturating the aqueous fluid flow with mineral ions. As soon as this fluid finds adequate thermodynamic conditions or there is a new increase in pH, the minerals will re-deposit, causing the scale phenomenon.

Figure 6 – Comparative aspects of the main oil recovery methods. (A) gas injection, (B) water injection and (C) water alternating gas injection (CO_2-WAG).

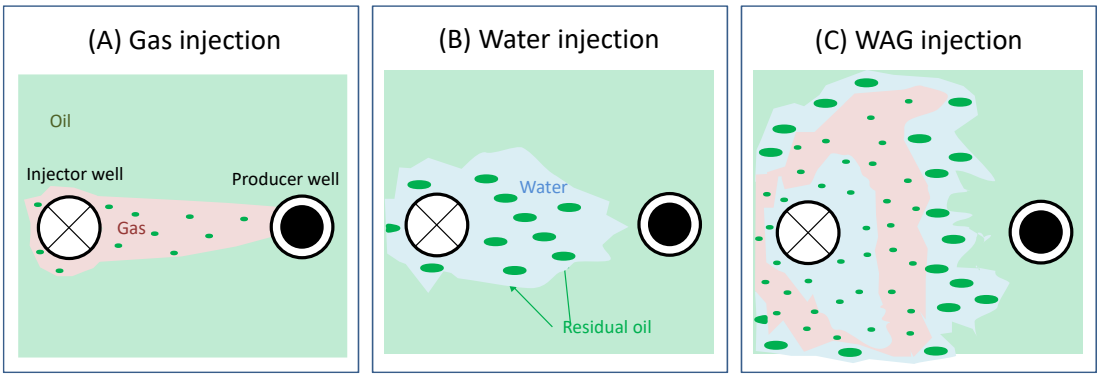

Source: created by the author.

2.3 **Impacts of oil mobility variation and scale on the productivity index**

The productivity index (J), defined by the ratio between the flow of the stream of interest in standard condition, normally the oil q_{os}, and the pressure variation of the flow in the considered drainage region, $P_e - P_w$, Equation (2), is usually used in the oil industry as a comparative parameter of productivity between wells and to monitor the behavior throughout their productive life. A drop in the value of J is a damage indication to the well or increase in the water saturation €n the drainage region, or even the combined effect of these two causes.

The right side of the Equation (2) can be deduced by applying Darc"s law and the pseudo-permanent radial flow Equation (1), Rosa et al. (2006). The expression shows that J can be expressed solely in terms of oil properties ($B_o, \mu_o, K_{ro(s_w)}$), of geometric parameters of the drainage system ($r_{w,}, h\ e\ r_e$), and the equivalent absolute permeability of the K drainage region, not depending on the characteristics of the elevation and surface systems. Figure 7 presents a description of the parameters used in equations (1) and (2).

Figure 7 – Main well parameters for flow estimation in the pseudo-permanent regime

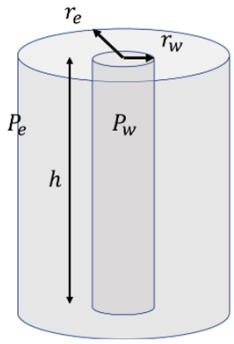

q_{os} Oil flow rate in surface condition
$K_{ro(s_w)}$ Relative permeability of oil in water saturation s_w
K Absolute permeability of the porous medium
h Length of open well to flow
$P_e; P_w$ Static pressure of the considered region and pressure in the well, respectively
B_o Oil formation volume factor
μ_o Oil viscosity under flow conditions
$r_e; r_w$ Radius of the considered region of the reservoir and radius of the well, respectively

$$q_{os} = \frac{2\pi K_{ro(s_w)} Kh(P_e - P_w)}{B_o \mu_o \, ln\,(\frac{r_e}{r_w})} \quad (1)$$

$$J = \frac{q_{os}}{P_e - P_w} = \frac{2\pi K_{ro(s_w)} Kh}{B_o \mu_o \, ln\,(\frac{r_e}{r_w})} \quad (2)$$

Source: created by the author.

2.3.1 Fluid effect

As can be seen from Equation (2), keeping all other parameters constant, J is directly proportional to the relative permeability of the oil $K_{ro(s_w)}$ and inversely proportional to the product of the oil formation volume factor by its viscosity $B\mu_o$. It so happens that, under normal operating conditions, with fluid pressure in the reservoir above the bubble pressure, the product $B\mu_o$ remains approximately constant throughout the productive life. The relative permeability to oil, however, is a function of the water saturation in the drainage region and significantly decreases with the progressive increase in water saturation in the region drained by the producer well, causing J to decrease for the oil phase. A relationship between the relative oil and water permeability curves $K_{ro(s_w)}$ versus $K_{rw(s_w)}$ is shown in Figure 8, s_{wi} is the irreducible water saturation.

Figure 8 – Example of relative permeability curves for oil and water as a function of water saturation.

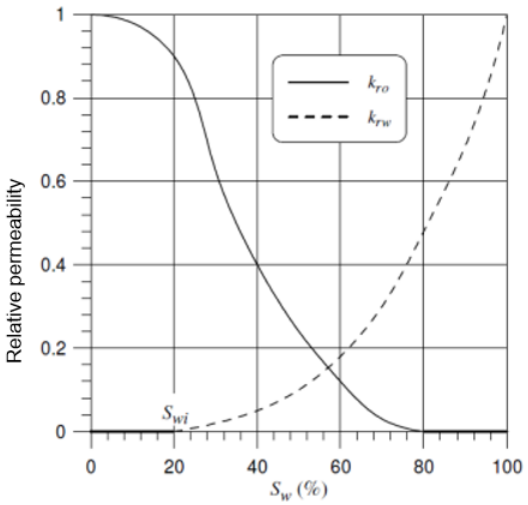

Source: Rosa et al., 2006.

2.3.2 Scale effect

Mineral precipitation from the reservoir in the vicinity of the well reduces the porosity of this damaged portion and consequently its absolute original permeability K to the damaged value K_d. On the other hand, scale removal operations or acid stimulation increase the permeability in the treatmen''s range of action, to the K_r value. Figure 9 shows a diagram of the drained regions of the reservoir still with original permeability (A), damaged (B) and with damage removal, or stimulated, (C).

Figure 9 – Permeability profile in the drainage region, (A) undamaged area, (B) damaged area and (C) area affected by the damage removal treatment or stimulation.

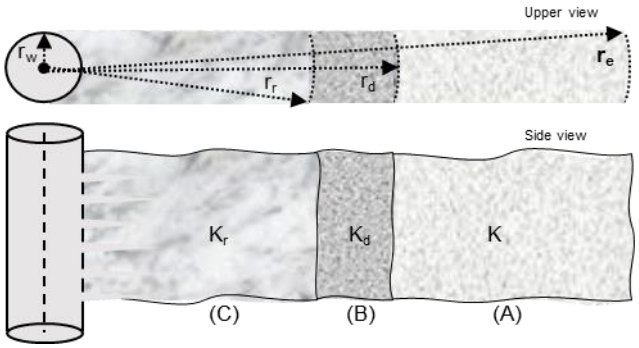

Source: Adapted from Fonseca, 2010.

The equivalent permeability of the drainage region in Figure 9 can be calculated using Equation (3) (Rosa et al., 2006).

$$K_{eq} = \frac{ln\frac{r_e}{r_w}}{\frac{1}{K}ln\frac{r_e}{r_d} + \frac{1}{K_d}ln\frac{r_d}{r_r} + \frac{1}{K_r}ln\frac{r_r}{r_w}} \quad (3)$$

2.3.3 Combined effect between K_{ro} variation and scale occurrence

From the above, both the occurrence of scale and the decrease in oil permeability occur with the arrival of water in the producer and both cause a decrease in J, making it impossible to separate these effects just by monitoring the productivity index during the production. This fact makes the diagnosis and quantification of the scale difficult, requiring the use of complementary analytical tools for this purpose, such as the compositional characterization of the fluids produced, with emphasis on the ionic characterization of the produced water; analysis of scale potential; monitoring of pressure loss in the production column and subsea lines; well logs during interventions, pressure tests during shut in; and the history of the well and other wells in the same field. Another approach in the assessment of scale in the reservoir that has been gaining ground is the incorporation of chemical models to the flow simulation (Flow Simulation with Reactive Transport). If the model is well adjusted, it can assess the specific effects of mineral deposition and of the variations in relative permeability on the productivity index.

2.4 Flow Simulation with Reactive Transport (FSRT)

In this dissertation, a FSRT model with the CMG-GEM compositional simulator was used to study the effects of mineral dissolution and deposition in the porous medium in a production scenario under the CO_2-WAG injection. However, the mineral deposition that most significantly impacts the productivity of wells is that which occurs in the vicinity of the perforations, because thermodynamic variations are more significant at the well-reservoir interface. This region is not well represented by the grid of simulation models, which commonly use cells with horizontal dimensions in the order of hundreds of meters. On the other hand, the significant deposition for the production occurs about tens of centimeters to a few meters of the perforations. One way to get around this dimensional difference would be to use a refinement of the entire grid, or a refinement located in the well region. Both approaches, however, have great difficulties. In the first case, the use of simulation grid with cells of the centimeters order to represent giant oil fields, as is the case of pre-salt fields, makes simulation unfeasible due to the high computational effort required, resulting in time prohibitive for the rounds, especially considering optimization problems. In the second case, a local refinement of order of 1:100

would be necessary, which generates great numerical difficulty for simulation, since large cells will be in contact with others with very small dimensions. To solve this problem, the present study proposes a proxy model that estimates the decrease in J caused by the scale deposited in the perforation region. This proxy is incorporated into CMG-GEM numerical model by creating simulator-specific triggers and is based on the composition of the fluids produced in a base simulation. This proxy uses the MultiScale (Kaasa, 2009), a prediction of mineral deposition software developed by EXPRO Petrotech Group, to calculate the precipitable mass in the region close to the perforations. Another proxy, also incorporated through triggers, emulates the effect of inhibition squeezes and complements the model. The proposed method is discussed in more detail in the methodology section. In the following paragraphs, some examples in the literature of the use of FSRT are presented, but none of them quantify the specific decrease in the productivity index caused by the localized scale in the perforation's well producers, in simulation models with large field scale.

Stamatakis et al. (2011) developed a tool that combines thermodynamics, kinetics, and hydrodynamics with one-dimensional flow to forecast precipitation of incrustation by $CaCO_3$ in the vicinity and inside producing wells. The development of the geochemical model was based on laboratory experiments on a small scale. Finally, the authors consider the main conditions for taking the results to the field scale:

a) Reliable thermodynamic model: The geochemical model should include a reliable thermodynamic model that can accurately predict the scaling tendency based on the chemical potential of scale formation.
b) Kinetic model: The model should incorporate a kinetic model that can predict the scaling rate based on the reaction rate of scale formation.
c) Transport model: The model should also include a transport model that can simulate flow in a porous medium, considering the flow and diffusion of electrolyte systems.

By considering these conditions, the geochemical model can predict the distribution of scale deposition along and around the production wells and the distribution of formation damage. This information can help engineers manage deposition and prevent formation damage in a timely manner.

Araújo (2012) evaluated the effects caused by rock-fluid interaction, in carbonate reservoirs, due to the injection of CO_2 and sea water, through the modeling of reactive transport with analysis of uncertainties of kinetic parameters. For this purpose, the work elaborated a flow model developed for the COORES simulator coupled to the ARXIM geochemical simulator, using COUGAR for the analysis of uncertainties. The results obtained indicated the

intense occurrence of dolomitization and dissolution of the rocks in the vicinity of the injection well. The water produced had a higher-than-expected calcium content, with a consequent increase in the potential for deposition of calcium salts in the reservoir. Despite the injection of large volumes of CO_2, the pH of the produced fluid remained close to the original values, due to reactions in a porous medium.

Novaes (2016) evaluated the injection of seawater without removing sulfate in carbonate reservoirs in Brazil, where desulphated seawater is commonly injected to prevent scale. The motivation was the greater efficiency and operational robustness of the injection without the removal of salt. The bypass of the removal system was simulated during the cleaning of the membranes, so that the system would not stop. To this end, a specific model for the simulation of reactive transport in a porous medium was developed in the COORES software coupled with the geochemical modeling of ARXIM. The results indicated that there was anhydrite precipitation in the reservoir, with the effect of decreasing the concentration of sulfate in the water produced, resulting in an increase in oil production. The temperature and magnesium concentration in the injection water were identified as the variables with the greatest impact on anhydrite precipitation. The results also revealed that there are no significant differences between an ideal continuous injection of desulphated sea water and the scenario studied with bypass of the sulfate removal unit during the periods of cleaning of the membranes.

Adegbite et al. (2017) studied the application of the Engineered Water Injection (EWI) method in advanced oil recovery. They investigated the recovery factor by comparing the geochemical effects caused by the injection water compared to the wettability effects. A model of multiple ion exchange reactions was developed to capture the effect of EWI in increasing the recovery factor in carbonates, and other geochemical reactions of rock-fluid interaction that commonly cause their dissolution and precipitation are also considered. With the results obtained, the authors believe that the change in wettability due to ion exchange is the main cause of the increase in the oil recovery factor.

Araújo et al. (2017) studied how the process of diagenesis took place in a carbonate sequence of the Quissamã formation, in the Campos Basin. For that, they used the CMG-GEM flow simulator with a compositional geochemical model of rock-fluid reactivity. The application simulated a period of 200 thousand years. The effects of dolomitization, carbonate cementation and rock dissolution were simulated, with and without fractures. The volume of circulated fluid was shown to be the most important factor for diagenesis among the variables analyzed.

Hajirezaie et al. (2019) proposes a method for studying Barite precipitation due to seawater injection using a 1 X 1 X 1000 cells model. The stud''s results showed that scale formation caused severe damage to the reservoir, resulting in reduced oil recovery and injectivity loss. Additionally, the study examined the scaling tendency and precipitation amount of different minerals in the wellbore based on water compositions from the Gulf of Mexico. It was observed that while some minerals precipitated in large amounts, others remained in equilibrium with the flowing brine. Furthermore, the findings indicated that maintaining a constant production flow requires a decrease in the bottom pressure of the producer well. These findings highlight the importance of considering mineral precipitation in reservoir management and water flooding operations. Effective scale inhibitors and strategies are necessary to mitigate the negative effects of scale formation. Further research is needed to develop models and techniques for managing scale formation in reservoirs and wellbores.

Rodrigues et al. (2019) developed a workflow based on FSRT to assess the impact that different choices of WAG parameters can have on oil recovery, scale deposition risk and CO_2 storage. The study was based on the sensitivity of the outcomes with the variation of four parameters: WAG ratio (proportion between the volumes of water and gas injected in each cycle), concentration of CO_2 in the injection stream, injection rate and solvent slug-size (percentage that the volume of gas injected in each cycle corresponds to the total porous volume occupied by hydrocarbons). The work was carried out in the scenario of injection of gas rich in CO_2 alternated with low sulfate seawater in carbonate type reservoirs. The authors identified that in this condition, calcium carbonate is the main mineral related to scale deposition and assumed the geochemical model with three aqueous reactions and one mineral reaction presented in Table 3.

All equilibrium constants (K_{eq}) in Table 3 are referenced to 25°C. The simulator used, CMG-GEM, utilizes Equation (4) to adjust the equilibrium constants to other temperatures throughout the flow in the porous medium.

Table 3 – Aqueous and mineral reactions present in the calcium scale mechanism.

$H_2O \leftrightarrow OH^- + H^+$	$(\log K_{eq} = -14)$
$CO_{2(aq)} + H_2O \leftrightarrow H^+ + HCO_3^-$	$(\log K_{eq} = -6.32)$
$HCO_3^- \leftrightarrow H^+ + CO_3^{-2}$	$(\log K_{eq} = -10.25)$
$CaCO_{3(s)} \leftrightarrow Ca^{+2} + CO_3^{-2}$	$(\log K_{eq} = -8.66)$

Source: Rodrigues et al. (2019)

$$K'_{eq} = K_{eq}.\exp\left[-\frac{E_a}{R}\left(\frac{1}{T'} - \frac{1}{298.15}\right)\right] \quad (4)$$

K'_{eq}	Equilibrium constant at temperature T'	K_{eq}	Equilibrium constant at 25ºC [=298.15K]
E_a	Activation energy [J/mol]	R	Gas constant [8.314 J / (mol K)]
T'	Current temperature [K]		

The workflow developed is applied to a small-scale pilot model with characteristics typical of the Brazilian pre-salt. The authors point out that the deposition of the Calcite scale is very sensitive to the reactivity constant used and the reactive surface area. As a result, the oil recovery factor is improved with the increase of the following parameters, in that order of importance: (1) concentration of CO_2 in the injection stream, (2) injection rate, (3) WAG ratio, (4) gas slug-size. The greater amount of CO_2 stored in the reservoir increased with the: (1) concentration of CO_2 in the injection stream, (2) WAG ratio, (3) injection rate (4) gas slug-size. The concentration of CO_2 in the injection stream proved to be the most important factor in the final recovery factor and in the greater storage of CO_2 in the reservoir, but it is strongly dependent on operational factors, being considered in the study as an uncertainty parameter and not as a variable of control. Despite the CO_2 injection concentration positively impacting the NPV due to the reduction of residual oil, and the CO_2 storage, it also resulted in a greater amount of rock dissolution and scale deposition, increasing the risk for the production. The study identified that WAG ratio values between 0 and 1, combined with slug-sizes between 1 and 8 months resulted in greater profitability. The risk of calcite deposition also increased with the increase in the WAG ratio.

Shabani et al. (2020) use the PHREEQC software to simulate a model that couples geochemical reactions with the reactive flow in a porous medium to study the increase in pressure difference, resulting from the formation of scale during water injection. The results of the difference in pressure and ionic concentration of the produced water agreed with three experimental results. The proposed model considered the different compositions of the injected and formation water, with their associated chemical reactions. The proposed method may, according to the authors, be used in the future to predict the decline in injectivity and for studies involving sensitivity analyzes.

Rodrigues et al. (2020) complement the work carried out in 2019 with the introduction of more parameters to the optimization process: the flow injection rates and the bottom hole pressure (BHP). As in the previous study, the objective was to determine the best design for

CO_2-WAG operations, considering economic aspects, occurrence of scale and minimization of environmental impacts related to CO_2 production. The authors structure the resolution method in two parts. In the first one, the optimization of the CO_2-WAG parameters is performed. The eight best solutions are identified according to a criterion that uses the trade-off between economic and environmental results. These solutions obtained in the first step are then used in the second part of the method, in which a reactive transport model is incorporated into the numerical model for the re-simulation of the solutions. With the simulated results and ionic compositions obtained in the second part, a risk assessment of the occurrence of depositions and flow assurance is carried out. For that, the authors determine the curves of the saturation index and calcium carbonate deposition potential through the scale prediction software ScαleFAST, developed in-house. The best design with rig campaigns for preventive treatment with inhibitor squeeze is then determined through modeling in the Squeeze 11 software and cost-effective considerations among the inhibition options for each scenario. According to the assumptions used by authors, however, the projected squeeze operations are always preventive and ensure that the well is inhibited throughout its entire productive life. Possible economic benefits of postponing squeezes to periods of decline in production, where the previous inhibition is no longer effective, were not evaluated. For this reason, the decline in production during the periods of deposition is also not estimated, nor is the inclusion of acid cleaning in the operations evaluated. Among the conclusions obtained, the authors note that allowing BHP variation improved the solutions obtained compared to the 2019 study. Another important conclusion is that CO_2 injection decreased scale precipitation potential, when compared to the case of waterflooding. According to the authors, this effect occurs in reservoirs with high levels of CO_2, in which the injection of water will react directly with the formatio''s CO_2, increasing the potential of scale in producing wells. Furthermore, as the scale is related to the aqueous phase, the production of higher water rates will contribute to a greater amount of deposition in the producers.

Azari et al. (2021) improve the methodology of Rodrigues (2020) with the implementation of a Gradient Descent algorithm with the objective of determining the size of treatments that results in the lowest cost and that guarantees that the producing well is always inhibited throughout its entire life cycle. The research identified that the optimal treatment corresponds to the inhibition of two million barrels of produced water, at each operation. The treatments, as in the previous work, are still performed in a totally preventive way and guarantee the producer's inhibition during the entire lifetime.

Reginato et al. (2021) also addressed EWI using numerical flow simulation, but replacing the simulato''s geochemical module, which has a high computational cost, with an artificial neural network (ANN) coupled to the simulator. The objective of the developed ANN was to enable the reproduction of the forecast of the oil and water production curves of the geochemical model by identifying the change in the relative permeability curves, which is caused by the different ionic concentrations between the injection water and the formation water. It was observed that the trained and validated ANN resulted in a reduction of simulation time by 90% when compared to the EWI geochemical modeling, which makes the use of the proposed methodology very attractive to optimization problems. After checking the quality of the ANN, the authors applied the method developed to optimize the NPV by identifying the best ionic concentrations of the injected water in a cutout of the UNISIM-II-D (Correia et al., 2015) model representing a quarter of a five-spot. The results of the best EWI configuration indicate a 49.62 million USD increase in NPV over seawater injection. It was also observed an increase in the oil recovery factor by 8.7% and a decrease in accumulated water production by 52%.

The present work is largely based on Rodrigues et al. (2020) but, contrary to this one, it seeks to quantify the impact that the occurrence of scale in perforations has on the oil production curve of wells, in addition to including acid cleaning treatments (with rig and remote) to the scope of operations. This approach makes it possible to include in the economic evaluation the performance of treatments in periods where the previous well inhibition is no longer effective.

3. METHODOLOGY

The objective stated in the introduction can be translated into solving a problem of optimizing the CO_2-WAG parameters and the periodicity of scale removal and inhibition operations, aiming at maximizing the NPV of hydrocarbon production. The expression for calculating the NPV, based on the Correia et al. (2020) proposal, with the addition of the term related to treatments (K_j . C_{trat}), is presented in equation (5).

$$NPV = [P(1-st)(1-r)\sum_{j=1}^{N}\frac{Q_{1,j}}{(1+t)^{j-1}} - \sum_{j=1}^{N}\frac{1}{(1+t)^{j-1}}(\sum_{i=1}^{5} C_i Q_{i,j} + K_j . C_{trat})]. (1-CR) \quad (5)$$

P	Oil price	t	Daily discount rate
st	Social taxes rates	i	Production/injection fluid stream i (produced fluids: 1–- oil, 2–- water, 3–- gas; and injected fluids: 4–- water; 5–- gas).
r	Royalties rate	C_i	Production/injection cost of fluid stream i
N	Total production days	K_j	Number of scale removal and scale inhibition treatments performed on day j
j	Production day j	C_{trat}	Treatment daily cost
$Q_{i,j}$	Daily production/injection low rate of fluid i on day j	CR	Corporate tax rate

The methodological proposal is to solve the exposed problem using an optimization application that controls the numerical simulations of compositional FSRT model. As this is a non-linear problem, with an unknown response surface, the optimization was carried out using heuristic solving methods. For this purpose, the CMOST optimizer software was used, with the selection of the DECE (Designed Exploration and Controlled Evolution) method developed by CMG. According to CMG-CMOST (2019), DECE is an iterative optimization process that initially applies an exploratory experiment design followed by a controlled evolution step.

The resolution methodology will be presented in two chronological phases of development. Both, however, with the same basic idea: the consideration in the FSRT of a well scale model and the optimization of CO_2-WAG and treatments parameters.

The results of the first phase were published in the SPE journal Production and Operation (Gomes and Sampaio, 2023). It is also intended to publish a new article with the results of the second phase.

The methodologies of the first and second phases differ in terms of the proxy used to calculate the precipitable mass and the number of steps in the optimization process, the second being an evolution of the first. Table 4 below summarizes the difference between the phases.

Table 4 – Main differences between the first and second methodological phases.

Methodology phase	Incorporation of the precipitable mass calculation into the FSRT	Optimization steps
First	Proxy with the accumulated volume of produced water	Two stages (1°WAG and 2° Treatments)
Second (improvement)	Proxy with ionic composition of produced water	A single integrated optimization step of all parameters

Source: Created by the author.

3.1 First phase of development

The resolution structure proposed in this work is presented in the flowchart of Figure 10 and consists of the following main steps:

1. Preparation of the FSRT model;
2. Choice of CO_2-WAG optimization parameters (reservoir pressure target and length of CO_2-WAG periods) and targets for performing treatments, which consist of the maximum allowable reduction of J before carrying out a treatment;
3. First optimization step: application of the CO_2-WAG optimization process with CMOST-GEM;
4. Determination of the precipitable mass curve: use of the chemical balance software MultiScale with the ionic composition of produced water and other parameters resulting from the first step (CO_2-WAG optimization);
5. Proxy preparation of the precipitated mass (MultiScale output) with the accumulated volume of produced water;
6. Second optimization step: with mass, scale and inhibition proxies, optimization is carried out to identify the best treatment periods;
7. Obtaining the best solution.

Figure 10 – Flowchart with the proposed method of resolution.

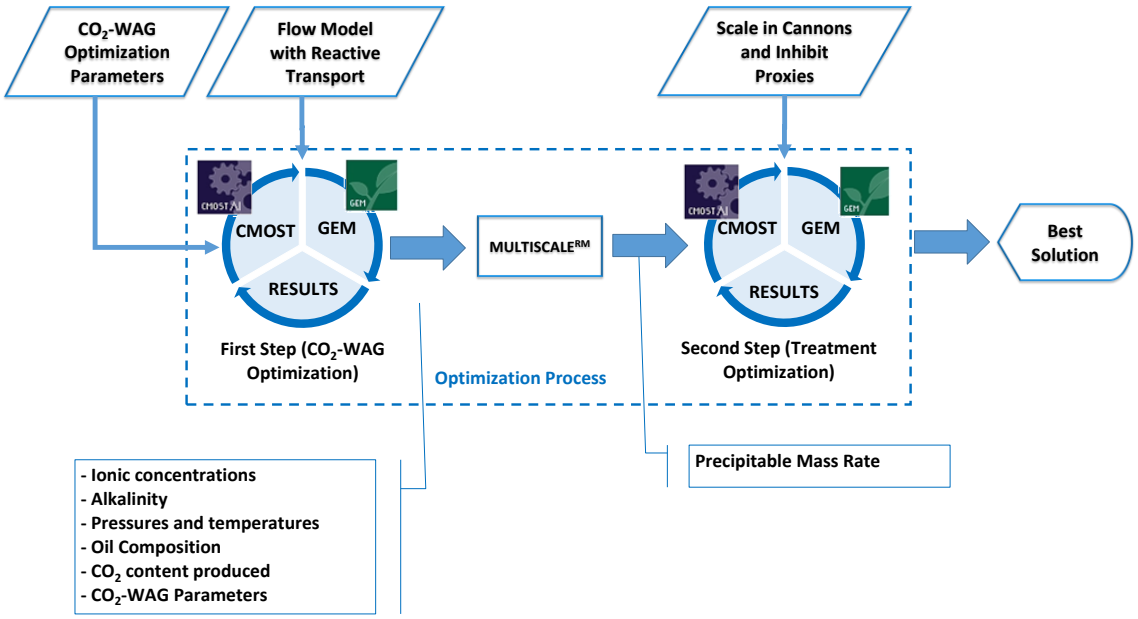

Source: created by the author.

3.1.1 Optimization and simulation process

The dynamics of the resolution takes place through two steps. The first consists of optimizing the CO_2-WAG parameters. The second step of the resolution consists of considering the incrustation in the region of the well perforations and searching for the best drop targets of the productivity index for treatments, for each range of water cuts. This step uses the set of best parameters obtained in the previous step and applies a proxy model that aims to provide greater detail for the region surrounding the perforations. The need to use two steps for the resolution is due to a problem of dimensional scale. The numerical model of the reservoir commonly has cells with horizontal dimensions in the order of hundreds of meters, while the region adjacent to the well, where the greatest thermodynamic variations occur and, therefore, more critical to the occurrence of deposition, is of the order of one meter. Thus, a horizontal grid refinement in the cells traversed by the well would have to be of the order of 1:100, which generates a lot of numerical instability and a significant increase in the simulation time, making its application to reservoir models prohibitive, especially regarding applications that involve the need for several simulations, such as parameter optimization. The second step aims to get around this numerical problem using proxies that emulate scale and inhibition in the vicinity of perforations.

3.1.1.1 First step of resolution–- optimization of CO_2-WAG injection parameters

The first step consists of optimizing CO_2-WAG parameters considering the occurrence of dissolutions and depositions that occur at field scale using a numerical simulation of FSRT model. The CO_2-WAG optimization is based on work of Sampaio et al., 2020 and Rodrigues et al., 2020, with the simplification of some assumptions and operating parameters to adapt to what was proposed by Correia et al. (2020). For this purpose, the absence of gas export was used as premise, which imposes the need for total reinjection of the gas produced and, therefore, that the contents of CO_2 and injected gas flows are equal to those produced. The use of two injection wells in the study cutout allows the continuous injection of water and gas into the model, even with the use of CO_2-WAG exchanges, so that when one of the wells injects water, the other injects gas.

The first step optimization parameters are:

Reservoir Pressure Target–- This parameter determines the volumes of water to be injected to maintain the target pressure.

Size of CO_2-WAG Periods–- this parameter determines the size of CO_2-WAG cycles in days. Each complete cycle is defined as the sum of the periods required to inject a slug of water plus the injection of a slug of gas. In this study it was considered that each slug of water or gas has the same number of days.

3.1.1.2 Second step of resolution–- optimization of scale removal and well inhibition treatments

This step seeks to find the best periods for the scale removal and inhibitor squeeze operations. For that, the best set up of parameters obtained in the first step are used, adding the scale and inhibition proxies of the perforation region. As a result, the best points for the treatment are obtained, after a certain previously stipulated number of 500 simulated experiments, with the design of experiments carried out by the DECE algorithm of CMG-CMOST.

3.1.1.2.1 Inhibit proxy

As expressed in the introduction, scale cleaning operations in wells commonly occur in conjunction with the application of scale inhibitors to the perforation region through the squeeze in the wells. The expectation is that the inhibitor will prevent the reoccurrence of scale for a certain period, usually until a certain volume of water is produced. The amount and

concentration of inhibitor designed for each treatment will define the expected accumulated volume of water production until the inhibition is no longer effective. This quantity, however, is quite limited to several conditions, such as costs and product inventory limit, product adherence to the reservoir rock, limited pumping and transport capacities, specific formulation for each well and maximum time for excess of product must be produced during treatment cleaning, to avoid product precipitation and consequent damage to the well. Therefore, the design of the inhibiting operation is specified for each well and will not be covered in this work. In the present study, a representative average inhibition was taken as a premise for all treatments that would prevent encrustation up to the accumulated volume of 300,000 m^3 of produced water. For this purpose, the sigmoid function presented in Equation (6) was used. This equation allows the estimation of the effect of inhibition f_{Inib}^{p} as a function of the accumulated volume of water produced ($Wp^p - Wp^t$) since the last squeeze of the product, on day t, until the simulated day of production p. The inhibitor is effective for value 1 and ineffective for value 0 of the function.

$$f_{Inhib}^{p} = \frac{1}{1 + e^{\left(\frac{Wp^p - Wp^t - 300{,}000}{1{,}000}\right)}} \qquad (6)$$

The profile of the function f_{Inhib}^{p} is shown in the Figure 11. It is observed that function rapidly changes from 1 to 0 when the accumulated volume ($Wp^p - Wp^t$) exceeds 300,000 m^3, value at which the inhibitor becomes ineffective ($f_{Inib}^{p} = 0$).

Figure 11 – Response profile of the sigmoid function as a function of the accumulated volume produced after each treatment ($Wp^p - Wp^t$).

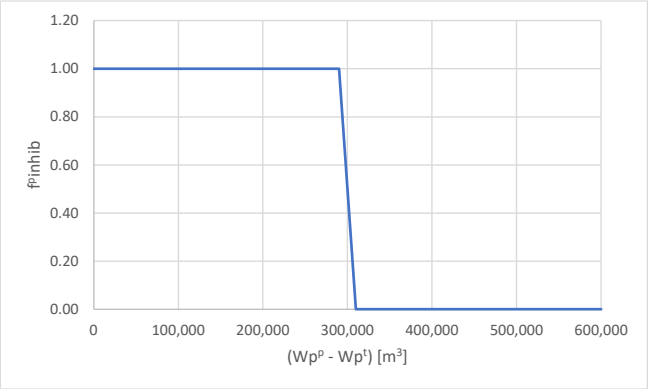

Source: created by the author.

3.1.1.2.2 Scale proxy

This proxy uses as input the time curve of the ionic composition of the produced water, obtained in the previous step for the optimized solution, and returns the time curve of the daily precipitable mass per m^3 of produced water, according to the saturation ratio calculated under the conditions pressure and temperature of the perforations. Based on these results, the reduction in porous volume in the vicinity of the well and the consequent decrease in absolute permeability is calculated using the Kozeny-Carman Equation (10). Finally, on each simulated day, the reduction of the productivity index J of the producing well is determined.

3.1.1.3 Calculation of precipitable mass and productivity index reducing factor (sr_{factor}^{p}).

Scale precipitation is related to the aqueous phase and depends on the ionic composition and aqueous volume of the water produced, in addition to the pressure and temperature of the study point. Through these properties, and the chemical balance properties of the species involved, such as reactive area, specific mass, scal''s saturation ratio and precipitable mass can be estimated. In this phase, the commercial software MultiScale was used to determine the precipitable mass per cubic meter of produced water, m. The Figure 12 below shows a schematic of the input parameters of MultiScale and the outputs of this deposition prediction simulator.

Figure 12 – Precipitable mass rate simulation using the MultiScale simulator.

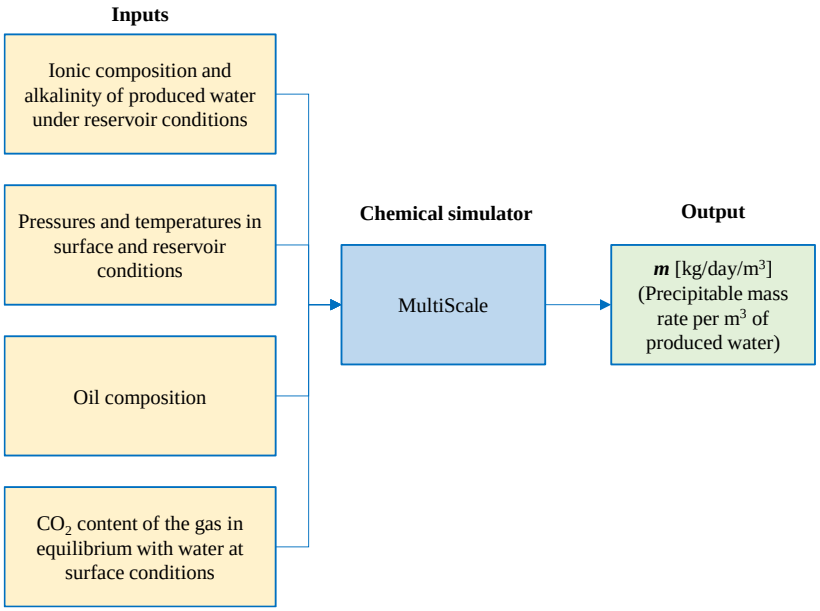

Source: created by the author.

In the result of the base simulation for MultiScale, it was observed that the ionic composition of the water did not vary significantly over periods of one year. For this reason, the calculation of the precipitable mass was performed based on the annual average values of the simulated parameters, resulting in an average precipitable mass rate per day and m^3 of produced water, m_j calculated at each simulated year j. The total precipitated mass, M_{tot}^{p}, in the production simulated day p is iteratively accounted by Equations (7) and (8), where q_w^p represents the daily water flow of day p and $f_{\text{Inhib}}^{p}$is the inhibition factor obtained by Equation (6). For production days t corresponding to the start of the simulation or reopening of the well after scale removal treatments, $M_{tot}^{p=t}$ is set as a part of the previously deposited mass and depends on the efficiency $efic_{Trat}$, Equation (6), considered for the treatment. If $efic_{Trat} = 100\%$ (full cleaning), $M_{tot}^{p=t}$becomes 0.

$$M_{tot}^{p\neq t} = M_{tot}^{p-1} + m_j.(1 - f_{Inhib}^{p}).q_w^p \tag{7}$$

And

$$M_{tot}^{p=t} = (1 - efic_{Trat}).M_{tot}^{p-1}, \quad for\ t \in \{0, days\ the\ well\ is\ opened, after\ each\ scale\ cleaning\} \tag{8}$$

The resulting effective porosity of the damaged region (see Figure 9) in day production p can be calculated through its porous volume ($\boldsymbol{\pi} r_d^2.H.\Phi_d^o$) , at the beginning of the simulation p = 0, discounting the total volume of deposited mineral (M_{tot}^{p}/ρ), until p day, and the result is divided by the bulk volume ($\pi r_d^2.H$). This calculation is presented by Equation (9). The parameter ρ represents the specific mass of the deposited mineral which, in the case study by this work, is Calcite ($\rho = 2730\ kg/m^3$).

$$\Phi_d^p = \frac{\pi r_d^2.H.\Phi_d^o - M_{tot}^{p}/\rho}{\pi r_d^2.H} \tag{9}$$

Knowing Φ_d^o, Φ_d^p, the ratio of permeabilities between day p and original, K_d^p/K_d^o is obtained by the Kozeny-Carman equation:

$$\frac{K_d^p}{K_d^o} = \left(\frac{\Phi_d^p}{\Phi_d^o}\right)^3 \cdot \left(\frac{1-\Phi_d^o}{1-\Phi_d^p}\right)^2 \qquad (10)$$

where $(K_d^o;\ \Phi_d^o)$ and $(K_d^p;\ \Phi_d^p)$ are the permeability-porosity pairs of the damaged zone, respectively original ($p = 0$) and in any production day p.

For simplicity, it is assumed that each treatment performed will reach the damaged radius ($r_r = r_d$, see Figure 13).

Figure 13 – Top view of the well and its drainage area, where (A) represents the general case and (B) the simplifying assumption r_r=r_d used in this study.

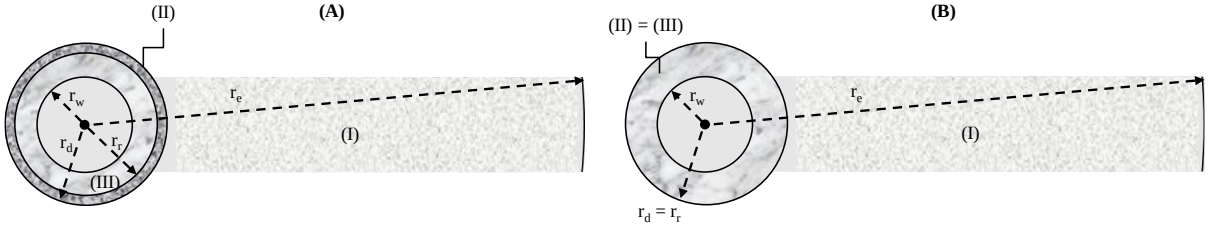

Drained regions of the reservoir:

(I) With original permeability

(II) Damaged

(III) With damage removal, or stimulated

Source: created by the author.

Therefore, taking Equation (3) and making the following substitutions $K_r = K_d$; $r_r = r_d$ and $K = K_{eq}^o$, the equivalent permeability of the considered drainage zone is obtained for every generic p, through the following expression:

$$K_{eq}^p = \frac{ln\frac{r_e}{r_w}}{\frac{1}{K_{eq}^o} ln\frac{r_e}{r_d} + \frac{1}{K_d^p} ln\frac{r_d}{r_w}} \qquad (11)$$

Dividing both sides of the previous expression by K_{eq}^o, making the substitution K_{eq}^o=K_d^o on the right side and arranging the terms of the expression, we obtain Equation (12) for the calculation of the equivalent permeability ratio of the drainage area. Equation (12) allows the calculation of K_{eq}^p/K_{eq}^o for the drainage area considered as a function of the permeability ratio of the damaged region K_d^p/K_d^o (see Figure 9) given by Equation (10).

$$\frac{K_{eq}^{p}}{K_{eq}^{o}} = \frac{ln\frac{r_e}{r_w}}{ln\frac{r_e}{r_d} + \frac{1}{\left(\frac{K_d^p}{K_d^o}\right)} ln\frac{r_d}{r_w}} \quad (12)$$

Finally, the reduction in the productivity index due to the occurrence of scale in the perforation region is determined using the expression (13).

$$sr_{factor}^{p} = \frac{J^p}{J^o} = \frac{K_{eq}^{p}}{K_{eq}^{o}} \quad (13)$$

The scale reduction factor sr_{factor}^{p} is updated at each timestep and passed to the GEM simulator, through the MULTO Keyword (CMG-GEM, 2019).

3.2 Second phase of development (improved methodology)

In this phase, an improvement of the applied method was sought through the development of a proxy to the chemical equilibrium software that directly correlates the precipitated mass with the ionic concentration of the produced water internally to the flow model, allowing for a more detailed calculation in real-time simulation using FSRT. This approach represents an enhancement compared to the previous development phase, in which the proxy was crudely made with the accumulated volume of produced water.

To enable the development of a high-quality expression that correlates the produced mass with the chemical concentrations of the water components, many rounds of the chemical equilibrium simulator are required under conditions close to those resulting from the flow simulator. For this reason, the use of Reaktoro (Leal, 2015) as the chemical equilibrium software was chosen, as it allows for the manipulation of a large amount of data using automation through the Python language, which was not possible with the MultiScale software used in the first phase.

Another point of improvement was the consolidation of the optimization process into a single step, allowing for the joint evaluation of potential parameter interactions that may impact the quality of the evaluated solutions.

With the described improvements, the methodology now follows the following steps.

1. Initial round of the flow model, using the produced water composition results, for each well and timestep, as input for the chemical equilibrium simulator, Reaktoro;

2. Simulation with the Reaktoro chemical equilibrium software using the base simulation results from the flow model, performed previously;
3. Determination of the proxy with an analytical expression that correlates the precipitated mass with the concentration of the components of the produced water, emulating the behavior of the chemical equilibrium simulator;
4. Incorporation of the adjusted proxy into the GEM flow model by triggers to calculate the precipitated mass at each simulation timestep for each producing well;
5. Incorporation of the scale and inhibition proxies developed in the first phase of the study (described earlier) into the GEM flow model;
6. Joint optimization of the CO_2-WAG parameters and the Treatment campaign to determine the best operational design.

The flowchart in

Figure 14 presents a schematic for the improved methodology of the second phase of development.

Figure 14 – Flowchart of the methodology for the second phase of development.

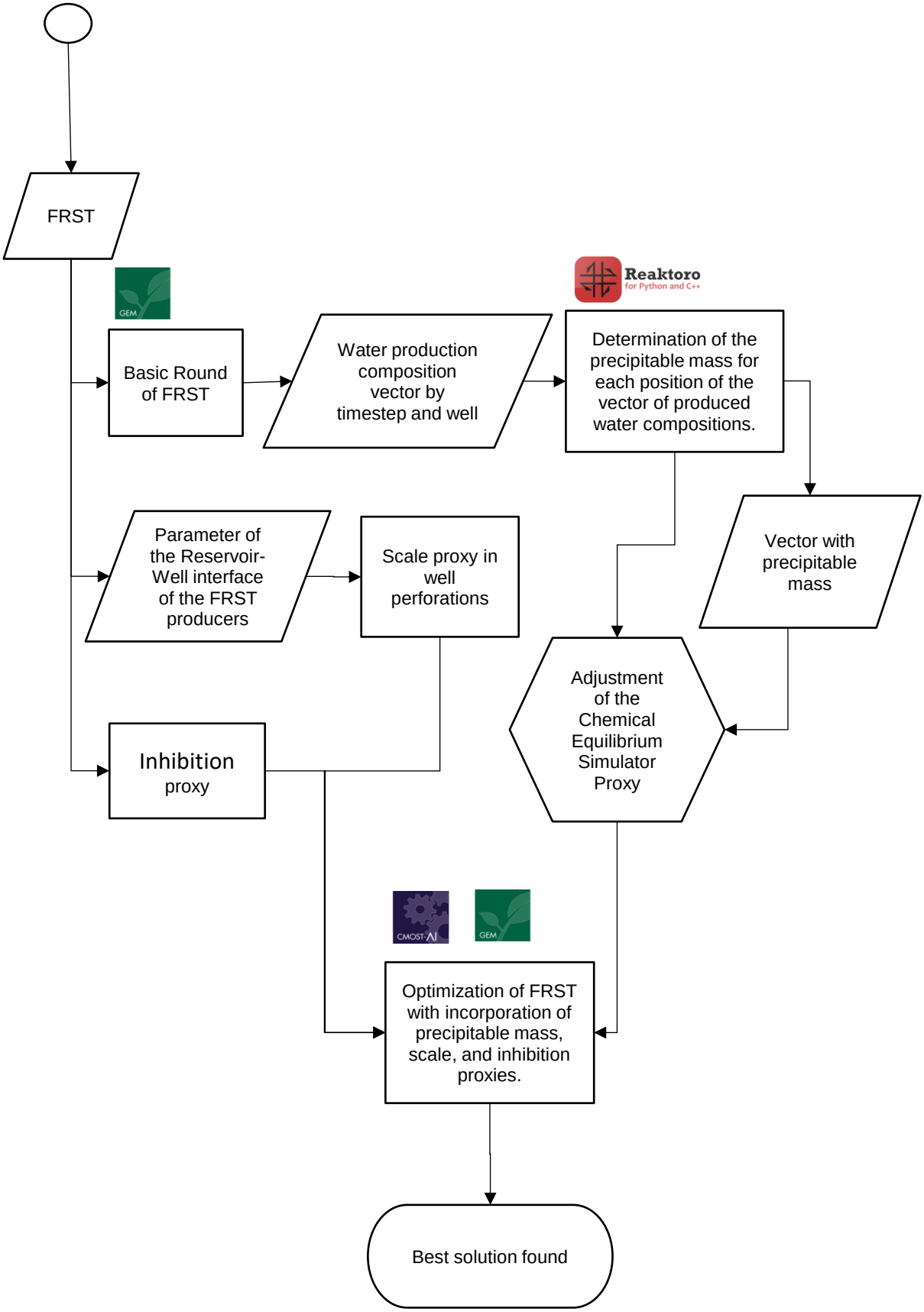

Source: created by the author.

4. CASE STUDIES

The methodology developed was applied to four case studies. The flow model used for application was UNISIM-III. This model was developed by researchers at the Center for Petroleum Studies (CEPETRO) at the University of Campinas and represents a carbonate, karstic and fractured field, with geological, fluid and heterogeneity characteristics of some fields in the Brazilian Pre-Salt (Correia et al., 2020). The fluid is characterized by its high CO_2 content and was modeled by CEPETRO based on the public Petrobras, 2015.

For cases 1, 2 and 3, a cutout of the UNISIM-III model was used with one producer and two CO_2-WAG injectors and the first phase development method was applied. For case 4, the complete UNISIM-III flow model was used, with simultaneous simulation of the operation of 6 production wells and 7 CO_2-WAG injection wells. For this case, the improved methodology of the second development phase was used Figure 15 below shows the complete UNISIM-III model, used for Case 4, and the position of the cutout extracted for application to Cases 1, 2 and 3.

Figure 15 – The complete UNISIM-III used in Case 4 and cutout used in Cases 1, 2 and 3.

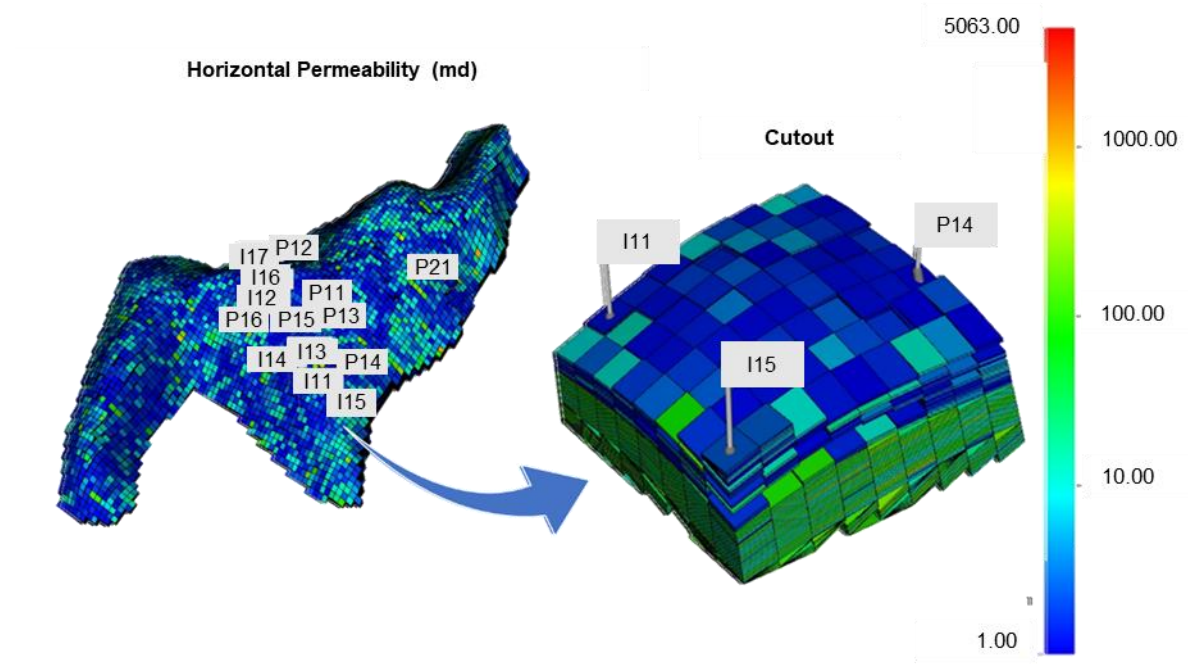

Source: created by the author.

Some characteristics of the cutout used are shown in Table 5.

Table 5 – Main features of the cutout and complete model used.

Property	Cuttout Model (Phase 1)	Complete Model (Phase 2)
OOIP (M3STD)	3.44E+07	1.71E+09
Number of blocks	8 x 9 x 309	63 x 120 x 309
Number of active blocks	6,260	234,528
Average Porosity (%)	8.28	9.63
Average Permeability x, y, z (md)	73.7 x 73.7 x 2.9	55.4 x 56.6 x 2.36

Source: Created by the author.

The fluid used in the UNISIM-III is modeled with five pseudo-components. The key characteristics of the fluid are presented in Table 6.

Table 6 – Main characteristics of the modeled fluid.

Parameter	Value
CO_2–- Gas (%)	44
CO_2–- Reservoir Fluid (%)	37
Reservoir Temperature	90
Psat (kgf/cm^2)	500
Initial Oil Visc. (cP)	0.39
GOR flash (sm^3/sm^3)	442
GOR dif. Lib (sm^3/sm^3)	604
GOR sep (sm^3/sm^3)	415
Bo sep (sm^3/m^3)	2

Source: Correia et al. (2020 apud Petrobras Report, 2015).

There are four facies represented in the used UNISIM-III model: Stromatolites, Karst Stromatolites, Coquinas, and Karst Coquinas. Each of these facies has a relative permeability oil and water curve represented in the graph of Figure 16. As can be observed in the graphs and according to Correia et al. (2020), the curves indicate a rock wettability between mixed and oil wet. In general, there is a higher mobility observed in the Coquinas facies compared to the Stromatolitic facies. The Karst facies exhibit significantly higher curves than the non-karstified facies, indicating greater fluid mobility.

Figure 16 – Relative permeabilities of oil and water for the facies in the UNISIM-III model.

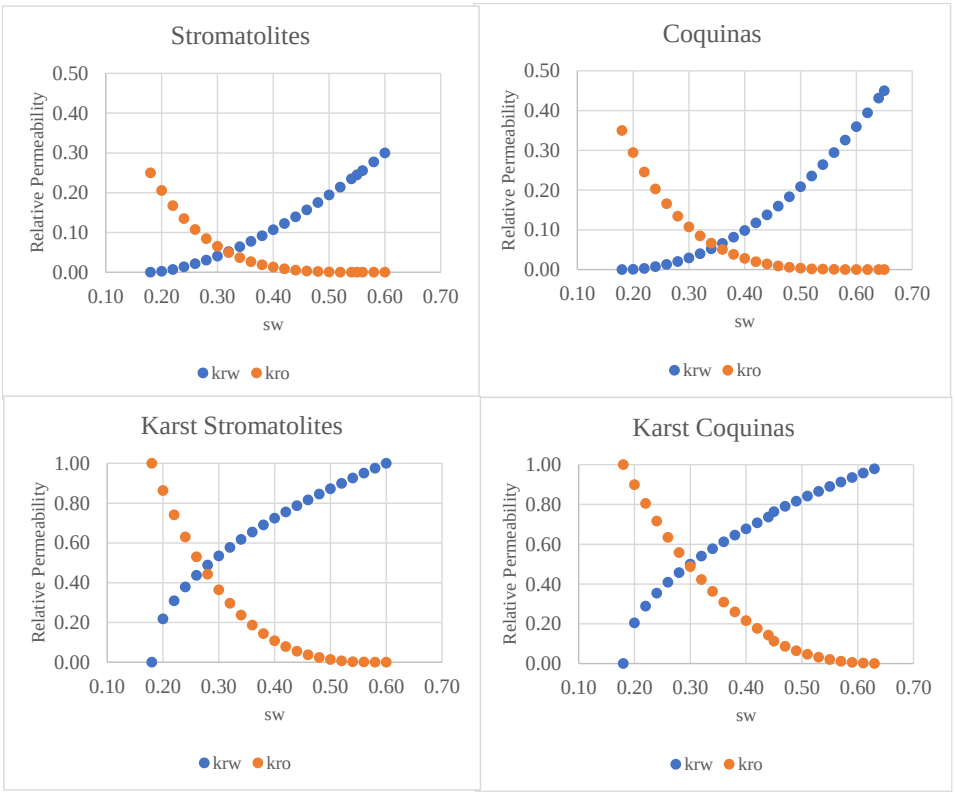

Source: Created by the author based on the UNISIM-III model.

Calcium carbonate is the most common scale in carbonate reservoirs with high CO_2 contents and under CO_2-WAG injection. For all cases, the chemical model used was extracted from Rodrigues et al., 2020 and is shown in Table 7. The composition of the reservoir was considered to be 90% Calcite, representing a simplified representation of a reservoir consisting of 80% Calcite and 10% Dolomite. The equations were introduced into the simulation model through the BUILDER preprocessor interface. The equilibrium constants and other chemical parameters used were generated using the BUILDER that, as mentioned in the Builder User Manual (CMG-BUILDER, 2019), incorporates the chemical libraries Phreeqc (Charlton et al., 1997) and Minteq.v4 (Allison et al., 1990).

Table 7 – Reactive chemical model of calcite precipitation and dissolution used in this study.

$H_2O \leftrightarrow OH^- + H^+$	(E1)
$CO_2\ (aq) + H_2O \leftrightarrow H^+ + HCO_3^-$	(E2)
$HCO_3^- \leftrightarrow H^+ + CO_3^{-2}$	(E3)
$CaCO_3(s) \leftrightarrow Ca^{+2} + CO_3^{-2}$	(E4)

Source: Rodrigues et al. (2019).

The compositions of the formation water and injected treated seawater (shown in Table 8) were also taken from Rodrigues et al. (2020). The composition of the injected water already considers the treatment to remove SO_4^{--} to avoid the souring effect in the reservoir (formation and production of H_2S) and corrosion of the productive systems.

The concentration of CO_2 for the formation water is indicated as zero in Table 8 because it is an initial setup. This value is updated by CMG-GEM in the first simulation time-step, considering the CO_2 from the equation of state (EOS) through its solubility in water (Henr''s model). The pH of the injection water is 7.72, slightly basic, while the pH of the formation water is acidic, with a value of 4.26. These values are representative of the pre-salt fields in Brazil.

Table 8 – Compositions used for injection and formation waters.

Concentration (ppm)		
Species	**Seawater**	**Formation water**
Na^+	12,285	45,028
Ca^{2+}	387.05	18,640
Cl^-	19,580	103,466
HCO_3^-	118.05	138.36
CO_2	1.53	0
H^+	1.85×10^{-5}	4.63×10^{-2}
OH^-	2.01×10^{-2}	8.75×10^{-5}
CO_3^{2-}	1.18	6.23×10^{-3}
TDS	32,372.77	167,272.62
pH	7.72	4.26

Source: Rodrigues et al. (2020).

Most of the economic variables used to calculate the NPV were extracted from Correia et al. (2020) and€S Markit (2022). In Table 9, parameters used in this work are presented.

Table 9 – Economic variables used in this work.

Variable / Parameter	Value
Revenues (USD/m³)	
Oil price (First Phase)	314.5
Oil price (Second Phase)	Table 10
Production Costs (USD/m³)	
Oil production	35.73
Water production	3.58
Water injection	3.58
Gas production	0.0096
Gas injection	0.0103
Unit Treatment Costs (MM USD)	
by Rig	4.53
Remote	2.18
Fiscal Assumptions (%)	
Corporate tax rate	34.0
Social taxes rates charged over gross revenue	9.25
Royalties rate	15.0
Other Parameters (%)	
Annual discount rate	9.0
Rig efficiency treatment	100
Remote efficiency treatment	80

Source: Adapted from Correia et al., 2020 € IHS Markit, 2022.

For the second phase of implementation, Case 4, the staggered price projection from Table 10 was used, based on the Brent projection (EIA, 2023).

Table 10 – Staggered price projection used in Case 4.

from year	to year	USD / M3STD
0	1	592.52
1	2	503.92
2	3	524.65
3	10	540.08
10	15	556.10
15	20	572.12

Source: Based on EIA, 2023.

The Minimum Miscibility Pressure (MMP) was estimated using the WINPROP software (CMG-WINPROP, 2019) at 40,880 kPa for the first contact and 40,151 for multiple contacts.

4.1 First phase of the application (cases 1, 2 and 3)

In the first phase of this study, corresponding to cases 1, 2 and 3, the methodology developed in the first phase of the research was applied to a cutout of UNISIM-III model with a producer well (P14) and two WAG injection wells (I11 and I15), which alternate the injection between gas and water. Two days of closed well were also considered to carry out each fluid change in the injectors, with the conversion of the water into the gas injector of the occasion always starting 2 days before the conversion of the gas into water injector, to avoid the interruption in the gas injection. To verify the effects of precipitation and mineral dissolution in the reservoir and scale in the p'oducer's perforation zone, three comparative studies were conducted. In each case, the CMOST optimizer generated 500 experiments simulated by the GEM (version 2019.12), with a simulated horizon of 27 years of production. For all cases, a cutout of the numerical model of a reservoir with compositional fluid UNISIM-III was used (Figure 15).

The injected water flows were conditioned to the maintenance of the Average Pressure of the reservoir at a value P_m chosen by the CMOST optimizer within the range of 50,000 to 70,000 kPa, in each simulated experiment.

The Botton Hole Pressure (P_w) for the producer was then defined as an optimization variable, being able to assume values in the range from 40,151 to 60,000 kPa, thus ensuring that the pressure in the reservoir is above the MMP pressure. This setting of the P_m and P_w variables guarantees the miscible displacement of hydrocarbons throughout the entire reservoir.

Table 11 presents the set of parameters used and the optimization ranges. The size of the CO_2-WAG cycles (SWC) corresponding to the time for a slug of water plus the time for a slug of gas, is chosen, for each experiment, in a range of 24 categories with 30 days each, ranging from 30.4 to 730.5 days. The time of each water or gas slug is constant throughout the simulation and corresponds to half of the SWC chosen by the optimizer in each round.

Table 11 – Well data and operational conditions.

Type	**Producer**	**WAG Injectors**
Maximum water rate (m^3 STD/d)	-	10,000
Maximum liquid rate (m^3 STD /d)	8,000	-
Maximum gas rate (m^3 STD /d)	-	4,000,000
Injector P_w (kPa)	(*)	Max 75,000
Optimization Parameters		
Type	**Minimum**	**Maximum**
Average Reservoir Pressure target – P_m_target (kPa)	50,000	70,000
Producer P_w (kPa)	40,151	60,000
SWC [Water + Gas] (days)	30	730
Period injected of each fluid [Water or Gas] (days)	SWC/2	

Source: Adapted from Correia et al. (2020).

The solubility of hydrocarbons in water is defined by Genera' Henry's Law (Harvey, 1996 and Li et al., 1986). For this work, the same coefficients of Sampaio et al., 2020 presented in Table 12 were used.

Table 12 – Coefficients and constants used in the hydrocarbon solubility model.

Pseudo-Component	**CO_2**	**N_2 to C1**	**C2 to NC5**
Henry Law Constants (kPa)	615,28.6	822,90.1	443,453.20
Infinite dilution coefficient (L/mol)	$3.18x10^{-2}$	$4.8x10^{-2}$	$6.8x10^{-2}$

Source: Based on Sampaio (2020).

Table 13 presents the setup of the parameters used in cases 2 and 3 for the scale proxy model. The original average porosity of the region under the effect of scale, Φ_d^o, was estimated in this work based on the cells penetrated by the well, but other estimators could also be used, such as porosity resulting from plug and core analysis, producer logging data or obtained from similar wells.

Table 13 – Parameters used in the well scale model (see Figure 9).

Parameter	Value	Unit
r_d	1	m
r_e	50	m
r_w	0.0889	m
P	2730	kg/m^3
H	244.15	m
Φ_d^o	0.1208	

Source: Created by the author.

4.1.1 Case 1 – only reservoir reactive model.

This case applies the chemical equations E1-E4 shown in Table 7, which consider dissolutions and precipitation in the reservoir. Inhibition and scale proxies that emulate the occurrence of scale in the produci'g well's perforation zone were not used and there are no treatment operations. Case 1 corresponds to the first step of the optimization methodology and aims to find the best setup for the size of the CO_2-WAG cycles (SWC), producer well P_w, and the average target for the reservoir P_m, which will define the volumes of water to be injected. The optimization ranges for this case are shown in Table 14.

Table 14 – Optimization ranges for Case 1 parameters.

Optimization Parameter	Minimum	Maximum
Reservoir pressure –arget - P_m (kPa)	50,000	70,000
Producer P_w target (kPa)	40,151	60,000
SWC (days)	30	730

Source: Created by the author.

4.1.2 Case 2 – full reactive model with rig treatment.

In this case, in addition to the application of the chemical reservoir model, inhibition and scale proxies were also used, which emulate the inhibition and occurrence of scale for perforation zone of the producing well. Rig operations are also considered for acid cleaning of scale, producer inhibitor squeeze, and well shutdown for 7 days during each combined treatment. For the P_m target and WAG cycle periods parameters, the results of the optimal solution of Case 1 were used. The specific parameters to be optimized in Case 2 are the J scale reduction targets ($sr^{target}_{wct\ range}$) for performing treatments. As it is expected that the attractiveness

of the treatments is linked to higher oil production and, therefore, lower water production, four water cut (WCT) ranges were defined for the optimization parameters $sr^{target}_{wct\ range}$:

a) sr^{target}_{1} : water cut greater than or equal to 0% and less than 10%;

b) sr^{target}_{2} : water cut greater than or equal to 10% to 40%;

c) sr^{target}_{3} : water cut greater than or equal to 40% to 60%;

d) sr^{target}_{4} : water cut greater than or equal to 60%.

Thus, when the values of sr^{p}_{factor}, calculated according to Equation (13), reach $sr^{target}_{wct\ range}$, for a given water cut value of the producer well P14 belongs to WCT range, a cleaning treatment and squeeze of inhibitor is performed.

4.1.3 Case 3 – full reactive model with remote treatment.

Same as Case 2 but considering remote treatments through the Stationary Production Unit (SPU), without using rig. Cases 2 and 3 represent evolutions of Case 1, adding to it the inhibition and scale proxies to determine how much the NPV is overestimated by not considerin' scale's effects in the producer well. In Case 2 the treatments are performed by rig considering 100% efficiency in the scale removal treatments and in Case 3 the treatments are performed remotely by the SPU with removal efficiency reduced to 80% for each operation cleaning, as it does not allow the use of flexible tube blasting, but at a lower operating cost.

4.2 Second phase of the application (Case 4)

After evaluating the behavior of phase 1 of the methodology developed on a reduced cutout of the field, in the second and final phase of the research, the improved methodology of the second phase of development was applied, in Case 4, to the complete UNISIM-III model. This case simulates the production for 20 years of 6 production wells (named P11 to P16) and 7 injection wells of the CO_2-WAG type (named I11 to I17), interconnected to a Floating Production Storage and Offloading (FPSO) type SPU. Given the significantly reduced cost of treatments performed remotely with the assistance of stimulation boats compared to treatments with rigs, only remote treatments were chosen for Case 4[1]. The gas produced, after subtracting the consumption, is reinjected back into the reservoir as there is no gas export. Just like in the previous cases, two days of closed injectors were considered to

[1] In the results chapter, a comparison of the Net Present Value (NPV) is presented for the cases of treatments using rigs (Case 2) and remote treatments (Case 3), demonstrating the advantage of the latter.

complete each CO_2-WAG fluid exchange operation, always starting with the water injectors of the moment to ensure the operational continuity of gas injection. For the exchanges, the wells were organized into clusters A and B, so that wells within the same cluster inject the same fluid simultaneously. The choice of clusters was based on visual clustering to achieve a balanced distribution of injected fluids in the reservoir. Figure Figure below shows cluster A, with wells circled in red (injectors I11, I12, I14, and I17), and cluster B, with wells circled in green (injectors I13, I15, and I16).

Figure 17 – Clustering of WAG injection wells in clusters A, corresponding to the injectors circled in red, and B, injectors circled in green.

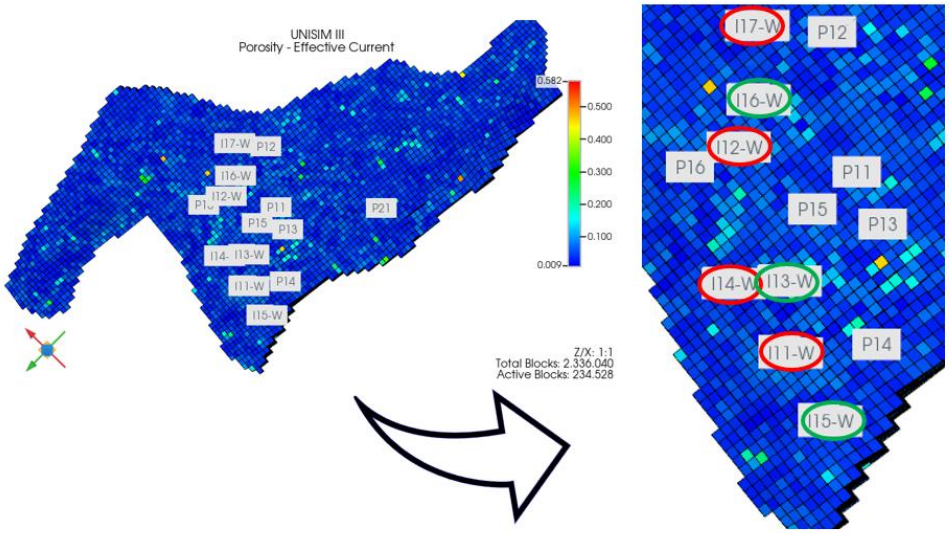

Source: created by the author.

Unlike previous cases where the precipitated mass correlated with the accumulated volume of produced water, in the improved methodology applied to Case 4, the proxy used for calculating the precipitated mass correlates the outputs of the chemical equilibrium software (Reaktoro) with the concentrations of the components in the produced water, determined based on an initial flow simulation (GEM). The idea is to obtain an analytical expression that can be easily introduced into the GEM flow model to enable real-time calculation during the optimization process. In addition to the proxy for calculating the precipitated mass, proxies for scale in the perforated zones and inhibition of the wells are also introduced into the flow model, as in previous cases.

Another point of innovation in the methodology applied to Case 4 is the single-step optimization process of the CO_2-WAG parameters and the treatment strategy, allowing for the

evaluation of possible interactions that may occur between the decision variables. The optimization parameters (decision variables) for Case 4 are presented in Table 15, along with their range of variation.

Table 15 – Optimization parameters for Case 4 and allowable ranges of variation.

Optimization Parameters	**Minimum**	**Maximum**
Reservoir		
Average reservoir pressure target – P_m_target (kPa)	50,000	70,000
Injection Wells		
SWC [water + gas] (days)	30	1461
Period injected of each fluid [water or gas] (days)	SWC/2	
Producer Wells		
Producer P_w (kPa)	40,151	60,000
Scale reduction targets for treatments (sr_i)	0%	100%

Source: Created by the author.

Before proceeding to the optimization process, individual parameters of the wells were computed in order to adjust the scale proxy for each well. The values of initial average porosity (Φ_d^o), open flow length (H), and mean drainage radius (r_e) were obtained from the UNISIM-III flow model using the Builder software (CMG-Builder, 2019). For all wells, a seven-inch diameter (0.0889 m) was adopted for the production casing and a mean radius of one meter for the region under the influence of calcite scale (specific gravity of 2,730 kgf/m^3). In addition to the scale proxy for each well, as in Cases 2 and 3, an inhibition proxy was also used, which prevents deposition until a volume of 300,000 m^3 of produced water is reached. Table 16 presents the parameter setup for the scale model for each well.

Table 16 – Parameters used in the well scale model for Case 4 (see Figure 9).

Parameter	**P11**	**P12**	**P13**	**P14**	**P15**	**P16**
r_d (m)	1	1	1	1	1	1
r_e (m)	39.68	39.17	39.61	41.55	39.23	39.77
r_w (m)	0.0889	0.0889	0.0889	0.0889	0.0889	0.0889
P (kg/m^3)	2730	2730	2730	2730	2730	2730
H (m)	335.84	373.24	307.54	246.60	316.96	182.26
$ø_d^o$ (%)	13.78	12.50	13.48	12.27	13.02	7.93

Source: Created by the author.

As Case 4 considers the simultaneous production and injection of multiple wells to the SPU, the capacity limits of the platform are of great importance for production management and optimization. Table presents the production capacities for oil, gas, and water, as well as gas and water injection for SPU.

Table 17 – SPU constraints.

Type	**SPU Capacities (M^3 STD)**
Maximum oil rate	28,617
Maximum liquid rate	28,617
Maximum water production rate	23,848
Maximum gas production rate	12,000,000
Maximum water injection rate	35,771

Source: Correia et al., 2020.

The optimization was conducted, as in previous cases, using the CMOST software, with rounds performed in the GEM flow simulator. The optimized solution was chosen based on the highest Net Present Value, Equation (5), obtained after 766 simulations conducted by CMOST. Since Case 4 is simulated in the full model while the previous cases are in the cutout, the simulation time for Case 4 is much longer than the time required for each round of the previous cases. Therefore, the decision was made to reduce the simulated horizon to 20 years (compared to 27 years in the previous cases). However, the extrapolation horizon of 20 years is still sufficiently adequate for the purpose of this study, considering that the magnitude of the contracts for product supply and service provision by the treatment boats is less than this period.

Figure 18 presents a schematic map of the cases studied in this work, including their assumptions, methodology, and the model used.

Figure 18 – Schematic of the case studies addressed in this work.

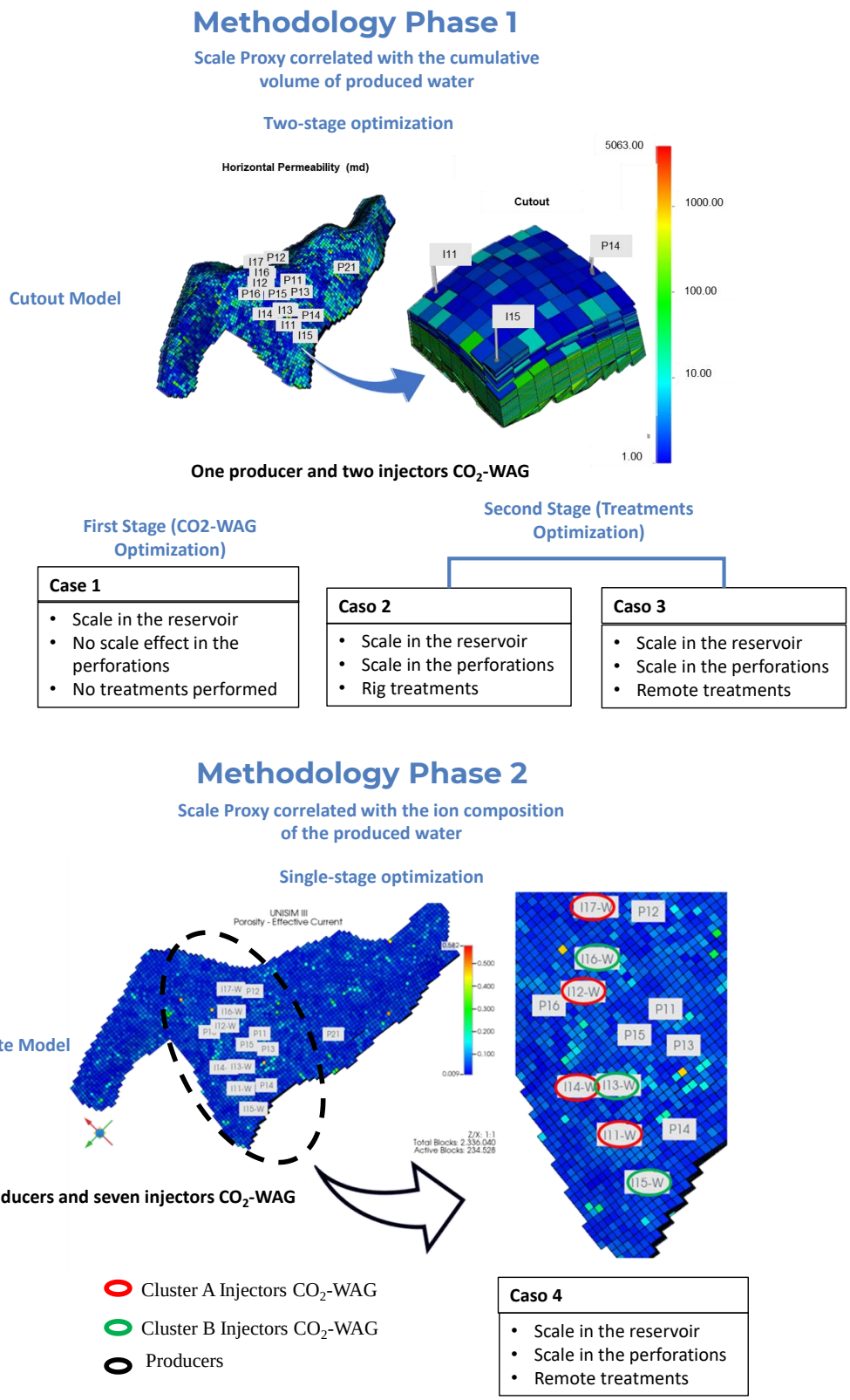

Source: created by the author.

5. RESULTS AND DISCUSSION

The results obtained will be presented in two parts. The first part corresponds to the cases related to the UNISIM-III model cutout and the application of the methodology developed in the first phase of the research (Cases 1, 2, and 3) which includes one producer well and two CO_2-WAG injection wells. The second part corresponds to the application of the improved methodology on the complete UNISIM-III model (Case 4) which includes six producers and seven CO_2-WAG injectors.

5.1 Results of the first part of the research

In this section, the results of applying the methodology of the first phase of development on a cutout of the UNISIM-III model will be presented. Three cases were studied for this purpose, with Case 1 corresponding to the CO_2-WAG optimization (first part of the optimization process). For the treatment optimization (second part), Cases 2 and 3 were studied. Case 2 considered treatments performed through well intervention rigs, while Case 3 focused on exclusively remote treatments.

The global simulation process (Case 1 + MultiScale + Cases 2 and 3) took about 43 hours in total to complete, using the launch of 10 simultaneous simulations at each optimization time step. Eight processing cores were used for each cutout simulation, with an average execution time of 20 min. The optimization of Cases 2 and 3 were performed simultaneously. The results obtained are presented below.

5.1.1 Results for Case 1

The Optimal Solution (OS) for Case 1 was found in experiment number 264. Although many other good quality alternatives were found, there was no improvement until the end of the simulations. For comparison basis, two cases were created, #1 and #2, with continuous injection of fluids in the injectors (without the use of CO_2-WAG exchanges). In the base Case #1, the injector I11 continuously injects gas and the injector I15 injects water. In the base Case #2 the wells inject the opposite fluids (I11 continuously water and I15 continuously gas). In both scenarios #1 and #2, the Gas Oil Ratio (GOR) threshold is reached, and production is stopped prematurely. In #1 production is stopped after 18.4 production years and in scenario #2 after 20 years, as can be observed in Figure 19b and Figure 19d. The OS found presents a significant increase in the NPV of nearly 60 million USD compared to the base Case #1, and 80 million USD compared to base Case #2, highlighting the importance of using the CO_2-WAG

strategy. Figure 19a shows the evolution of the objective function and the points that represent the OS obtained and the NPV of cases #1 and #2. As can be seen, most of the solutions using CO_2-WAG result in higher NPV than #1 and #2.

Figure 19b shows the cumulative NPV time series for #1, #2 and OS. It is observed that in the first years of production, solutions #1 and #2 present higher values of accumulated NPV than OS, especially solution #2. This result is due to elevation effects given by the better gas-liquid ratio of solutions #1 and #2, in this period. However, in the long term, the greater production of water and gas of #1 and #2 (Figure 19e and Figure 19f), in addition to causing undesirable production costs, impact on the reduction of oil production (Figure 19d). From the 11th year of production, OS emerges as the solution with the highest NPV, standing out more and more from #1 and #2. The OS shows an increasing trend even at the end of the simulation period, indicating that it is economically viable to continue production beyond the 28-year horizon. It can be observed, respectively, in Figure 19e and Figure 19f, that the production of water and gas from the OS is significantly lower than that of the solutions that do not use the CO_2-WAG method, as expected, with a later breakthrough, which impacts on the higher production of accumulated oil at the end of the OS. The total volume of oil produced of 12.2 MM^3STD for the OS represents a recovery factor of 35.3%.

The graph in Figure c presents the evolution of the WAG injection ratio (WAG Ratio) between water and gas in reservoir condition and per injection well over the 41 CO_2-WAG cycles performed by the OS, and the relationship of this parameter with the average pressure of the reservoir. Initially, with the reservoir pressure significantly above the target of 59,400kPa, less water is injected, and the WAG Ratio results in values less than 1. After a transient period of oscillation, the average reservoir pressure stabilizes, and the WAG Ratio becomes close to 1.

Figure 19 – Outputs for Case 1. (a) evolution of the objective function for Case 1; (b) NPV timeseries for OS, #1 and #2; (c) evolution of the WAG ratio over the cycles (d) cumulative oil production timeseries for OS, #1 e #2; (e) water cut timeseries for OS, #1 and #2; (f) gas oil ratio timeseries for OS, #1 and #2.

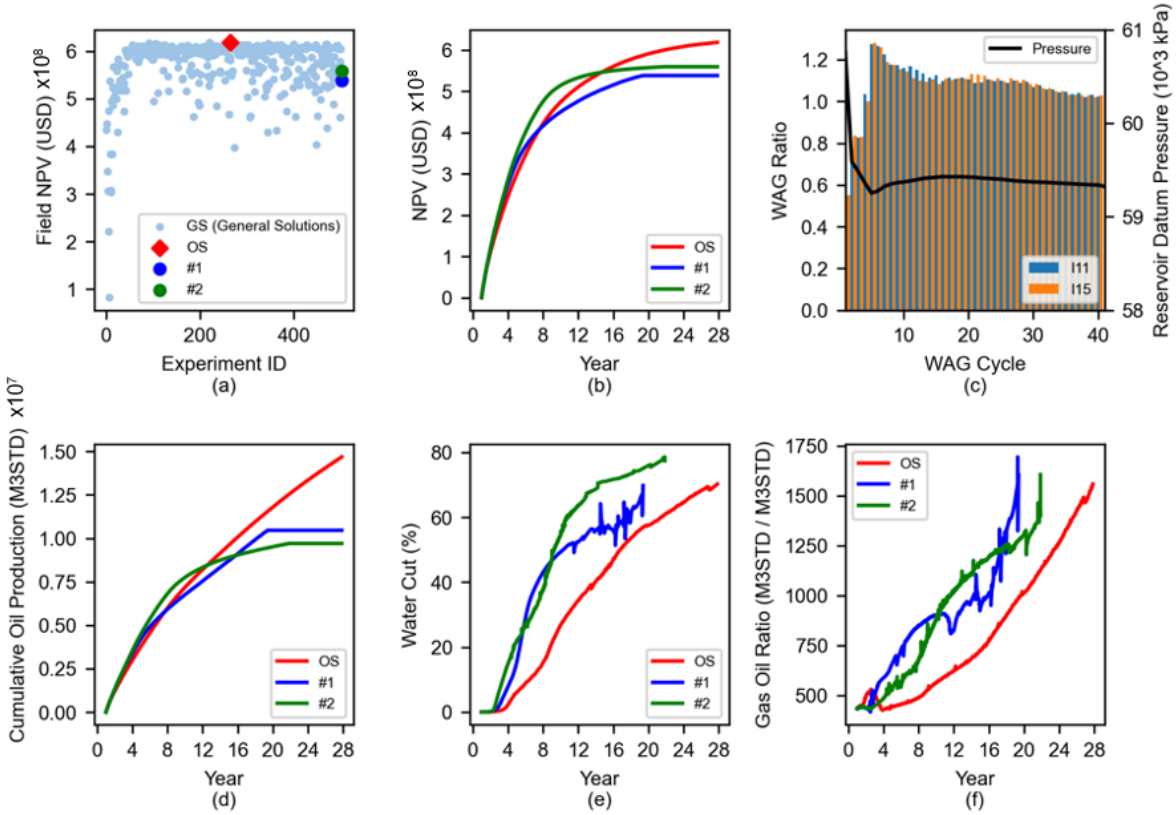

Source: created by the author.

Table 18 presents the setup of the simulated parameters and the resulting NPV for the Optimal Solution and for the comparative Case #1 and Case #2.

Table 18 – Optimized parameters found for Case 1 and the resulting NPV.

Experiment	SWC (days)	P_m Target (kPa)	Producer P_w Target (kPa)	Resultant NPV (million USD)
Optimal Solution	244	59400	40449	618
Case #1	---	59400	40449	558
Case #2	---	59400	40449	537

Source: Created by the author.

The Figure 20a presents the ionic concentration curve of the produced water as a function of the cumulative volume produced. The values obtained from these curves were used as input for the MultiScale simulator to determine the curve of the average daily rate of precipitable mass per cubic meter of produced water m_j, in bottom well condition. It is observed that the concentration of Na^+ and Cl^- ions drops along the production, which happens due to the

arrival of the injection water, of lower salinity, in the producer. An increase in bicarbonate concentrations in the produced water is also observed, indicating a greater reactivity of the produced water with the breakthrough of the injection water. On the other hand, the concentrations of calcium and carbonate did not vary significantly, probably due to the attainment of equilibrium of the injected water with the reservoir rock, along the flow in a porous medium. Calcium carbonate is at the solubility limit under the average conditions of the well drainage area, with the excess already deposited in the reservoir. However, under the pressure and temperature conditions of the bottom of the well, this salt becomes supersaturated, and calcium carbonate tends to be deposited as indicated in Figure 20b, which shows the m_j curve (in red). The M_j curve (in black) corresponds to the total precipitable mass per day and is obtained by multiplying m_j by the flow rate of produced water. It is observed that the values of M_j are quite significant, indicating that the results obtained for Case 1 should be overestimated due to the non-consideration of scale's effects on the producer. As discussed in the methodology, the m_j curve will be used to calculate the reduction of the productivity index J in cases 2 and 3, which consider the effect of scale on the producer well.

Figure 20 – (a) Curves of ionic molality of produced water; (b) total scale precipitable daily mass (M_j) and per cubic meter of produced water (m_j).

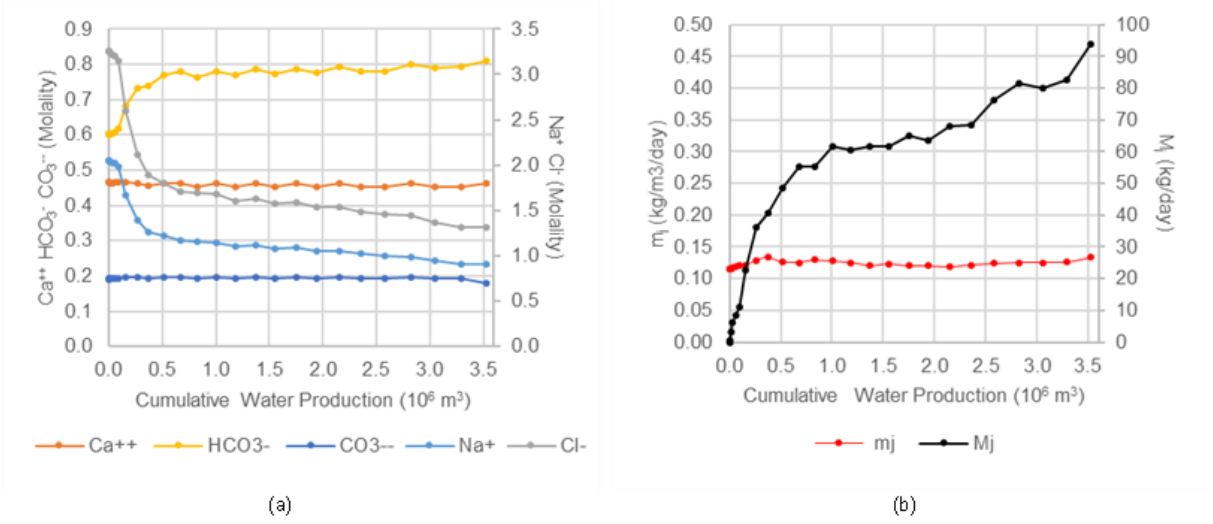

Source: Created by the author.

Figure 21a, and Figure 21b shows the profile of the total dissolved or precipitated mass in the section between injectors I11, I15 and producer P14, at the end of production. The negative values (in shades of blue) represent the portions of the reservoir where there was

dissolution and the positive values (in shades of red) the portions where there was precipitation of calcite. It is observed that dissolutions occur mostly in the vicinity of the injectors with very high intensity, greater than a ton of dissolved mass scale, on the other hand, occur throughout the entire reservoir, intensifying a little in the producer's region (dark red cells).

Figure 21 – Profile of the total dissolved or precipitated mass: (a) in the section between injector I15 and producer P14, and (b) between injector I11 and producer P14.

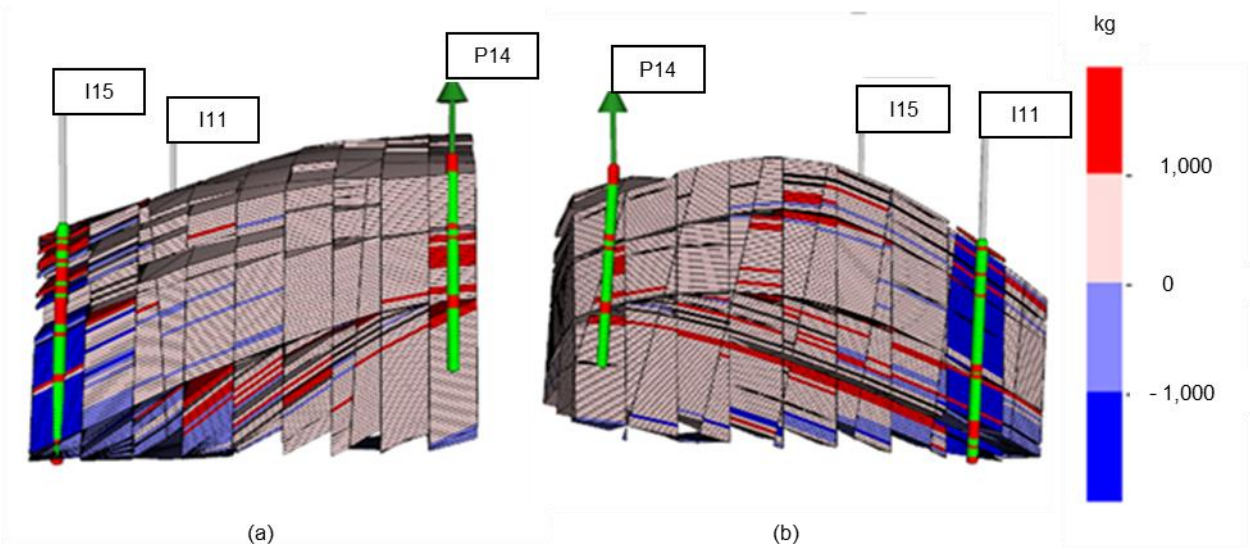

Source: Created by the author.

5.1.2 Results for Cases 2 and 3

For cases 2 (rig treatment) and 3 (remote treatment) the well scale model was applied using the value of 59,400 kPa as a fixed target for the reservoir pressure, 40,500 kPa for the producer's P_w and 244 days for the period of the CO_2-WAG cycles, all parameters obtained in the optimal solution of Case 1 (first step). Figure 22a and Figure 22b shows the evolution of the objective function for cases 2 and 3, respectively. In Case 2, the best solution was found in experiment number 395 and in Case 3, in experiment 324.

For comparison purposes, treatments performed always preventively were also simulated, for each case, with rig (Case 2) and remote (Case 3). The expressive gain obtained with a proposed approach to identify the optimal point for performing the treatments can be seen in the graphs in Figure 22. The optimal solution for Case 2 resulted in the NPV of US$ 559 million, this value represents a gain of 41.3 million USD (8%) in relation to the scenario of always preventive treatments. For Case 3, the NPV for OS was 570 million USD, an increase

of 13 million USD (2.3%) in relation to the remote treatments performed always preventively, a relative smaller difference due to the operational costs being lower than those of Case 2.

Figure 22 – Evolution of the objective function for: (a) Case 2 – rig and (b) Case 3 - remote.

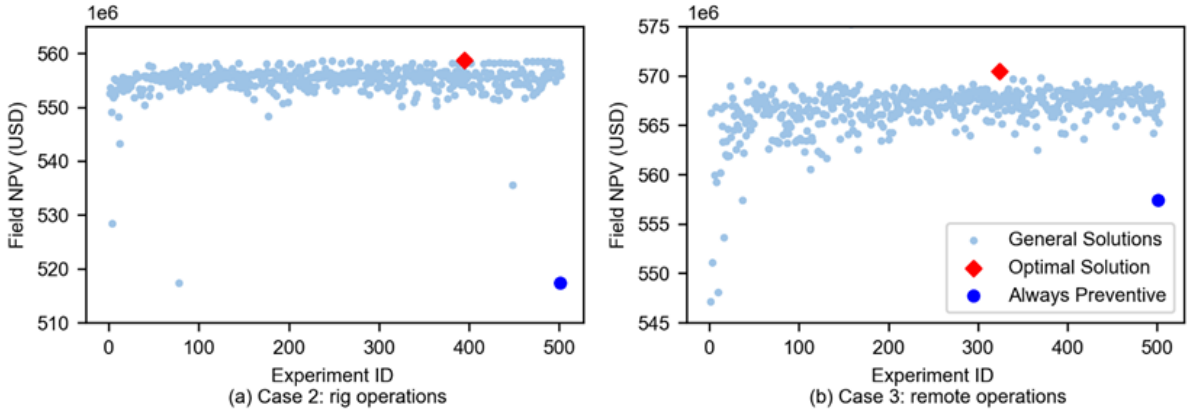

Source: Created by the author.

Table 19 presents the configuration of parameters in the optimal solution, the result of the objective function and the number of resulting treatments for each case. It is observed that the lower efficiency of Case 3 (remote) compared to Case 2 (rig), according to Table 9, is offset by the lower costs of remote operation, which allows for a greater number of treatments to be carried out, resulting in a NPV of 11.7 million USD higher for remote treatment. As expected, in the optimized solution, the $sr^{target}_{wct\ range}$ decrease with the increase in water cut, showing the decrease in the attractiveness of the treatments with the increase in water production. In general, the results indicate that in the rig option there is an increase in economy in the treatment later than in the remote option. The comparison of the solutions indicates that it is economically more interesting to invest in the adequacy of the SPU to carry out remote treatments than the use of rigs for these operations.

Table 19 – Input parameters of the Optimal Solution for Cases 2 and 3 and resulting outputs.

	Optimal Solution Inputs							**Outputs**	
	Reservoir Pressure Target (kPa)	**Producer P_w Target (kPa)**	**WAG Cicle Period (days)**	**sr_1^{target}**	**sr_2^{target}**	**sr_3^{target}**	**sr_4^{target}**	**Number of Tratments**	**NPV (million USD)**
Case 2	59,400	40,449	244	1.00	0.91	0.56	0.28	7	559
Case 3	59,400	40,449	244	1.00	0.92	0.81	0.18	9	570

Source: Created by the author.

Figure 23a shows the temporal profile of the number of treatments. Although the start of water production occurs around the 4th year, treatment takes place only around the 9th year. This is due to the inhibition effect and lower water cut values in the initial years. Due to the lower costs for the operations, 9 treatments were performed in Case 3, two more than in Case 2.

Figure 23 b and c show, respectively, the time series of the oil production flow rate and water cut for cases 1, 2 and 3. The evolution of the water cut is very close for both cases 2 and 3, and it is slightly higher for case 1. It is observed that for water cut values from 0 to 40%, the treatments are performed as soon as the producer is no longer inhibited (as in preventive mode) and practically at the same time for cases 2 and 3. This is due to the high attractiveness economy arising from the high production of oil during this period. With the increase in water production, however, treatments tend to be postponed in both cases. In general, it is also verified that the postponement is greater for rig treatments (Case 2) due to their higher cost. However, for water cuts above 60%, the result was reversed, with the postponement of the remote treatment, which occurred due to the influence of the production time limit on the optimization process. Figure 23b shows that, during the moments when treatments are performed and inhibition is effective, the productivity of cases 2 and 3 returns to be very close to the production curve of Case 1. This result indicates the effectiveness and importance of performing the treatments. However, the losses incurred during the period when the inhibition is no longer effective are not recovered.

A comparison of the cumulated NPV time series for the cases is shown Figure 23d. Until the 7th production year, the curves are very close due to the low water production, from then on, the curves with the scale model in the well (cases 2 and 3) begin to move away from Case 1. Cases 2 and 3 starts to stand out from the 11th production year onwards. Although the curve in Case 1 has the highest cumulative NPV, this is not realistic, as it does not consider the potential for the scale of the water produced in the bottom hole condition, which will lead to the formation of scale in the perforation zone and decreased productivity. Considering the best strategy found with the application of the scale model in the producer well, which is the remote treatments (Case 3), the resulting NPV for Case 1 will be overestimated at about 48 million USD. For the purposes of evaluating the importance of treatments, Case 1* was included in the graph of Figure 12d, which is the same as Case 1 with the addition of the scale proxy, but without performing treatments. This case resulted in an NPV of 515 million USD. This value is 44 million USD lower than the result for case 2 (rig treatments) and 55 million USD lower than case 3 (remote treatments), evidencing the importance of treatments.

Figure 23 – Timeseries for outputs best solutions: (a) number of treatments for cases 2 and 3; (b) oil production rate for cases 2 and 3; (c) water cut for cases 2 and 3; (d) evolution of NPV for all cases.

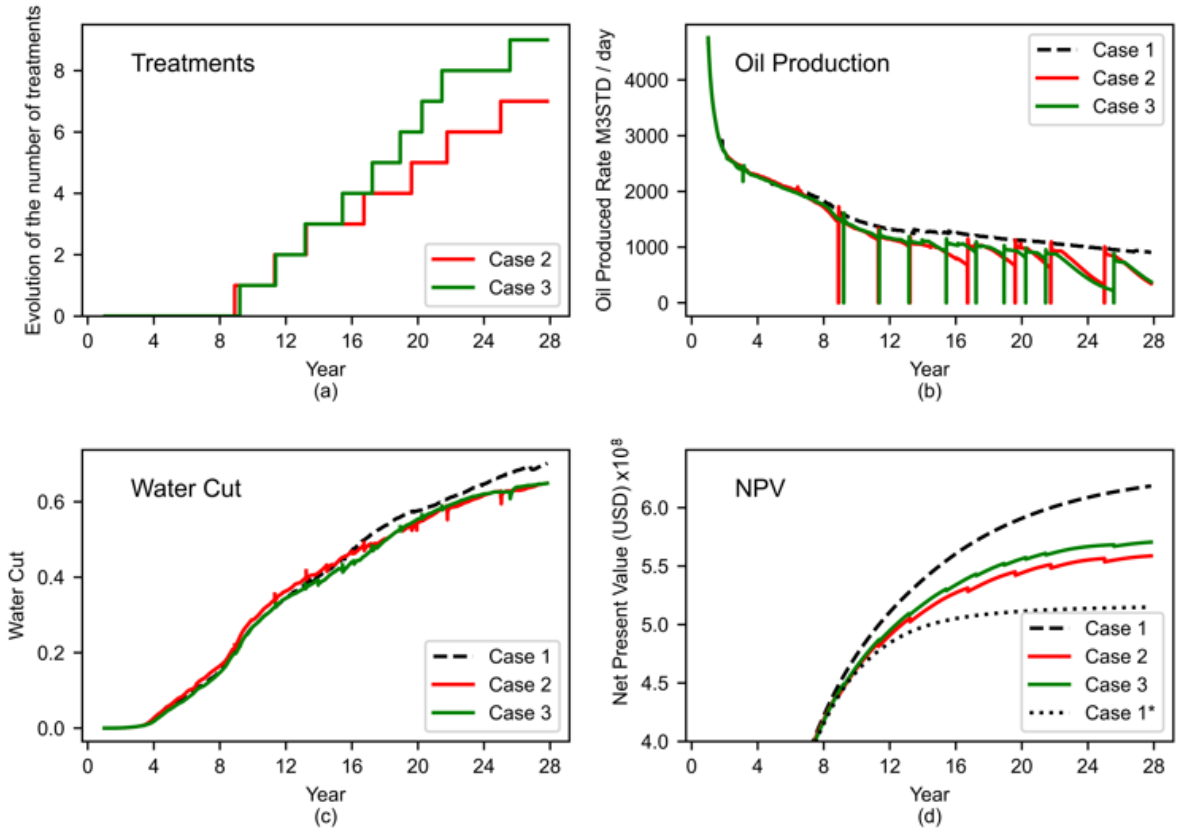

Source: Created by the author.

The results of this first part of the research were published in the journal SPE Production & Operation (Gomes and Sampaio, 2023).

5.2 Results of the second part of the research

The second phase of the research studied the behavior of the joint production of six producing wells and the fluid exchanges of seven CO_2-WAG-injectors, all connected to a SPU in a representative pre-salt carbonate field subject to scale occurrence (Case 4).

5.2.1 Characteristics of the application in Case 4

The improved methodology from the second phase of development was applied in Case 4. This improvement is mainly characterized by allowing a more accurate calculation, in flow simulation time, of the precipitated scale mass through the calibration of a proxy from the chemical equilibrium simulator results with the ionic concentrations of the produced water. Another methodological improvement is that, unlike the previous development phase, the

optimization process is carried out in a single step, considering all variables related to CO_2-WAG and treatment design together, which allows for the verification of possible interactions of these variables in the same process.

5.2.2 Adjustment of the proxy for the calculation of the precipitable mass.

The proxy for the precipitable mass corresponds to an analytical expression obtained from the results of the chemical equilibrium simulator with the results of a previous simulation of the flow model, FSRT, used as a base. In this initial base flow simulation, the reactive model module of GEM is applied to the complete UNISIM-III. Since the objective is to gather time series of the ionic compositions of the produced water, the initial model does not consider the scale effect in the wellbores, and therefore, there are no treatments (the scale and inhibition proxies are disabled). For the adjustment of the proxy, a simulation horizon of 28 years was used in the flow simulator. Figure 24 presents the time series obtained for the concentration of the produced ionic species resulting from GEM.

Figure 24 – Time series of produced ionic species concentration from GEM simulation (input for Reaktoro).

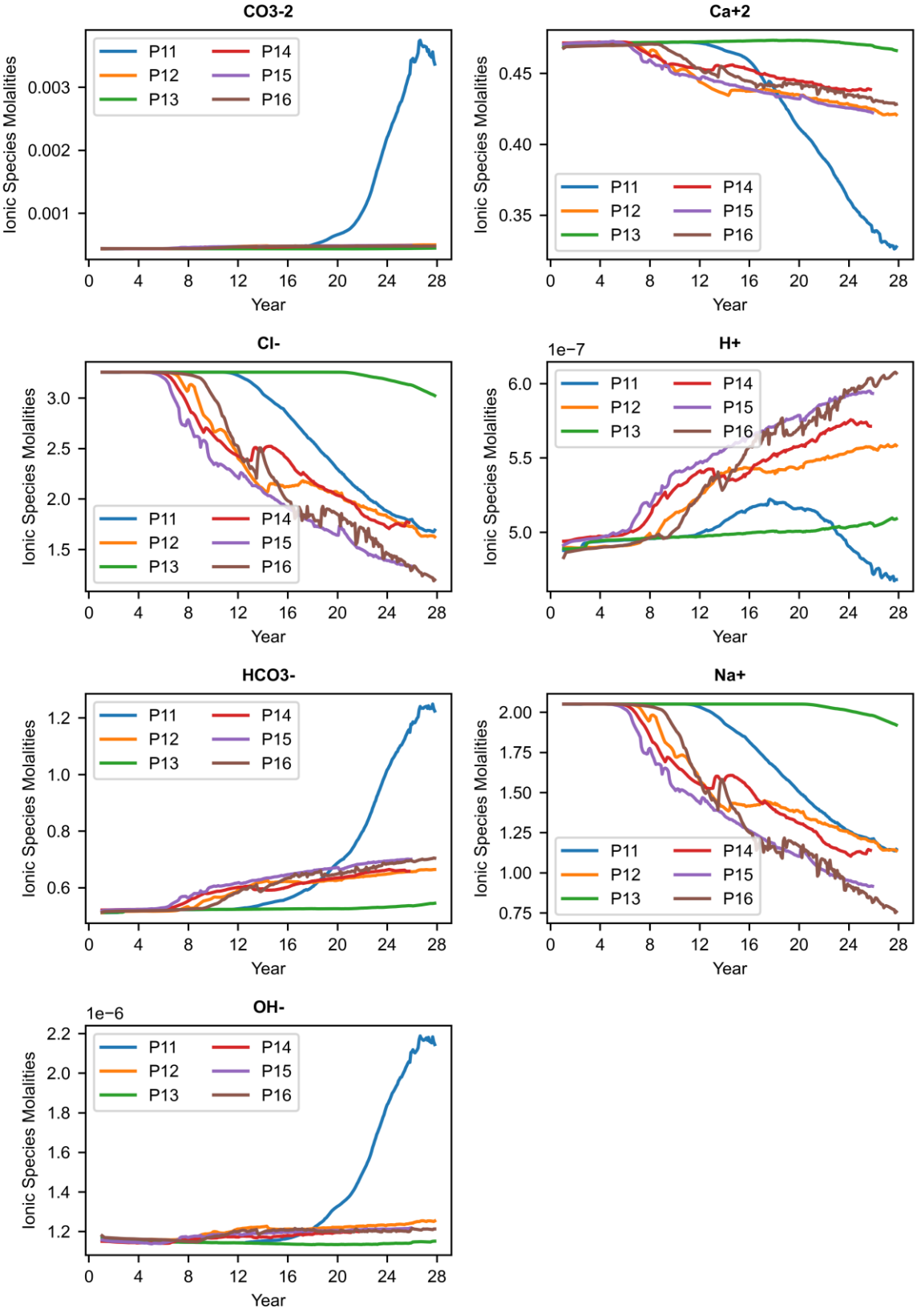

Source: Created by the author.

In Figure 24, it can be observed that, despite a general dispersion of the results, there is a similar trend in behavior among the wells, especially in the early years of production extrapolation, when some wells begin to deviate from the general trend. For carbonate [$CO3^{-2}$], most wells maintain the concentration of this ion in the produced water around 5e-4 Molal throughout the horizon, except for well P11, whose concentration starts to increase significantly around year 16, along with the concentration of bicarbonate ion [$HCO3^{-2}$]. Although the increase in bicarbonate is more strongly observed in well P11, the increase occurs analogously in the other wells, except for well P13 where the increase is more gradual. Consistent with the increase in bicarbonate ion, there is a reduction in calcium ion [Ca^{+2}] in all wells. This behavior is typical of wells at risk of calcium carbonate scale. In the concentration graph of [H^{+}] ion, the increase can be observed in most wells throughout the horizon. Well P11 is the only one that reverses this increasing trend starting from year 16, when the concentration of [H^{+}] starts to decline and maintains a downward trend until the end of the simulation horizon, a behavior again consistent with the significant increase in carbonate ion around that year. In contrast to the other wells, the significant increase in concentrations of [OH^{-}] also indicates, along with bicarbonate, an increase in well alkalinity from year 16 onwards. Well P13 showed the least variation in ion concentrations during the entire simulated horizon. The relatively constant concentrations of [Na^{+}] and [Cl^{-}] for P13 indicate that there was no significant influx of injection water in this producer, which explains the limited variation in the other ionic concentrations of this well that predominantly produces formation water throughout the horizon. For the other wells, there is an increase in the volumes of injected water over time, indicated by the decrease in salinity [NaCl]. This effect of mixing formation water and injection water is the main cause of the strong ionic variation in these wells.

The concentration data were then input into the chemical equilibrium simulator Reaktoro. This simulator allowed for the control of a large number of simulations experiments through automation using the Python language (1868 chemical equilibrium points were simulated). Table 20 presents the statistical result for the linear regression between the simulated ionic concentration points and the Reaktoro result.

Table 20 – Statistical Results for Linear Regression between Simulated Ionic Concentrations and Reaktoro Results.

Regression Statistics								
Multiple R	0.997							
R-Squared	0.995							
Adjusted R-Squared	0.995							
Standard Error	0.002							
Observations	1869							
ANOVA								
		df	**SS**	**MS**	**F**	**Significance F**		
Regression		8.00	1.94	0.24	43023	0.00		
Residual		1860.00	0.01	0.00				
Total		1.95						
	Coefficient	**Std Error**	**t stat**	**P-value**	**95% Lower**	**95% Upper**	**Lower 95%**	**Upper 95%**
Intercept	-2.1E-01	5.6E-02	-3.8E+00	1.2E-04	-3.2E-01	-1.1E-01	-3.2E-01	-1.1E-01
$CO3^{2-}$	-1.4E+02	2.2E+00	-6.3E+01	0.0E+00	-1.4E+02	-1.3E+02	-1.4E+02	-1.3E+02
Ca^{2+}	-4.9E-01	4.6E-02	-1.1E+01	1.6E-25	-5.8E-01	-4.0E-01	-5.8E-01	-4.0E-01
Cl-	5.1E-02	3.6E-03	1.4E+01	6.3E-43	4.3E-02	5.8E-02	4.3E-02	5.8E-02
H+	4.2E+05	8.0E+04	5.2E+00	2.6E-07	2.6E+05	5.7E+05	2.6E+05	5.7E+05
HCO^{3-}	5.1E-01	2.5E-02	2.1E+01	1.2E-84	4.6E-01	5.6E-01	4.6E-01	5.6E-01
Na^{+}	-2.3E-02	5.1E-03	-4.6E+00	5.5E-06	-3.3E-02	-1.3E-02	-3.3E-02	-1.3E-02
OH^{-}	1.5E+05	2.2E+04	6.9E+00	9.6E-12	1.1E+05	1.9E+05	1.1E+05	1.9E+05
BHP	-1.5E-08	5.3E-08	-2.9E-01	7.7E-01	-1.2E-07	8.8E-08	-1.2E-07	8.8E-08

Source: Created by the author.

In Table 20, the regression statistics indicate a high level of correlation between the simulated and Reaktoro data, with a multiple R^2 of 0.997 and an R-squared value of 0.995, suggesting a strong linear relationship between the variables. The ANOVA table provides information on the significance of the regression model. The F-statistic of 43023 and its associated p-value of 0.00 indicate that the regression model is statistically significant. Moving on to the coefficients, each variable's coefficient estimate, standard error, t-statistic, and p-value are provided. The intercept has a coefficient of -2.1E-01, indicating a negative relationship with the dependent variable. The $CO3^{-2}$, Ca^{+2}, Cl^{-}, H^{+}, HCO^{-3}, Na^{+}, and OH^{-} ions show negative coefficients, while the BHP (Bottom Hole Pressure) coefficient is not statistically significant. The coefficients' t-statistics and associated p-values suggest that the variables $CO3^{-2}$, Ca^{+2}, Cl^{-}, H^{+}, HCO^{-3}, Na^{+} and OH^{-} have statistically significant relationships with the dependent

variable. The 95% lower and upper bounds indicate the range within which the true population coefficients are likely to fall.

The results of the statistical analysis indicate that the precipitable mass obtained from Reaktoro, under the boundary conditions of the flow simulation, can be accurately estimated using the linear regression defined by the coefficients in Table 20.

Figure 25 visually presents the relationship between the results from Reaktoro and the ones calculated using the individually applied proxy defined by linear regression, highlighting the excellent quality of the proxy for everyone well.

Figure 25 – Visual relationship comparison: Reaktoro results vs. linear regression proxy for individual wells.

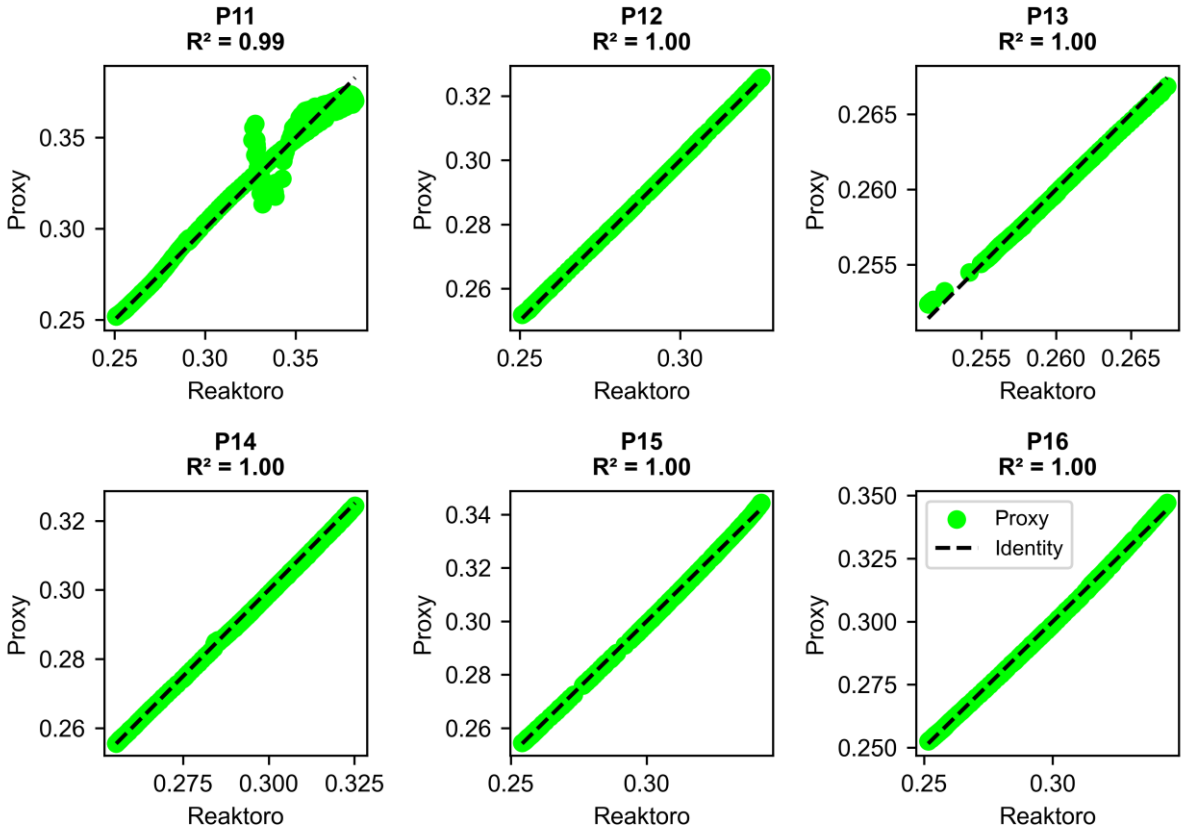

Source: created by the author.

For well P11, despite the proxy still being quite representative with an R-squared value of 0.99, there are points that are visibly further away from the identity line. The analysis of the results indicates that these points were obtained after the 20th year of production, precisely when the slope of the bicarbonate concentration curve starts to become more pronounced compared to the behavior of the other wells (Figure 24). As presented below, the optimization

process was defined with a horizon of 20 years. The graph in Figure 26 shows the same points as Figure 25 for well P11 but excluding the points with production beyond the 20th year. For these points, the same proxy defined by regression over 28 years was able to estimate the Reaktoro results with excellent precision.

Figure 26 – Reaktoro Results vs. linear regression proxy for production data from the first 20 years of well P11.

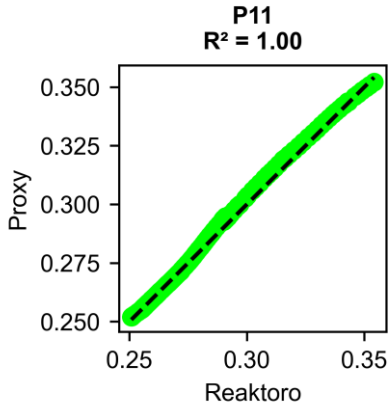

Source: created by the author.

5.2.3 Results of the optimization process

Once the precipitable mass proxy was defined, it was introduced into the UNISIM-III model of GEM, initiating the optimization phase aimed at finding the best setup for the parameters (related to CO_2-WAG and treatments), considering the precipitation effect on perforations and treatments (proxies for scale and inhibition).

For comparison purposes, cases #1 and #2 were also simulated, with continuous injection of fluids in the injectors (without the use of CO_2-WAG exchanges). In case #1, the injectors in the cluster A (red outline on the map in Figure 17) continuously inject water and the injectors in the cluster B continuously inject gas (green outline on the map in Figure 17). Case #2 represents the inverted condition in relation to the previous case, with the injectors of Cluster A injecting only gas and those of Cluster B injecting only water throughout the simulated horizon.

In addition to the previously mentioned cases #1 and #2, which involved continuous injection of fluids without CO_2-WAG exchanges, three more cases were considered. Case #3 considers treatments that are always performed preventively at the point where the previous

inhibition becomes ineffective. Case #4 represents the scenario where no treatments are performed. Additionally, case #5 does not consider the occurrence of scaling in the perforations.

For all comparison cases, the optimization parameters were assigned the same values as the optimal solution (OS), except for the CO_2-WAG exchange period in cases #1 and #2 (where no exchanges occur). The ideal points for IP reduction treatments were adjusted in case #3 (always performed preventively) and case #4 (where treatments are not allowed). In case #5, the scaling proxy in the perforations was disabled. Table 21 summarizes the comparison cases with the optimal solution (OS).

Table 21 – Comparison cases summary

Comparison Cases with OS	Description
#1	Without CO_2-WAG exchange, with cluster A (wells I11, I12, I14 and I17) always injecting water and cluster B (I13, I15 and I16) always injecting gas.
#2	Without WAG exchange with the situation inverted compared to #1 (cluster A always injects gas and cluster B always injects water).
#3	Treatments always performed preventively, at the exact point where the inhibition performed by the previous treatment ceases to be effective.
#4	No treatments are performed. As in previous cases and OS, the effect of scale in the perforations is considered, however, there is no cleaning and inhibition treatment carried out.
#5	Unlike previous cases and the OS, the occurrence of scale in the perforations is not considered. As a result, the production results are overestimated.

Source: Created by the author.

The complete optimization process in Case 4 took a total of 260 hours to complete. The optimization was conducted with the simultaneous launch of 45 simulations chosen by CMOST at each step of the process. As in previous cases, eight processing cores were used in parallel for each simulation, which resulted in an average execution time of 13 hours per simulated job.

Figure 27 shows the evolution of the objective function results for the obtained solutions, with a focus on the OS and the resulting NPV for comparison cases #1, #2, #3, #4, and #5 (highlighted as colored points plotted at the end of the graph). Table 22 presents the NPV value obtained for each case, as well as the difference in NPV between each comparison case and the OS.

Figure 27 – Evolution of the objective function for the OS and NPV of the comparison cases.

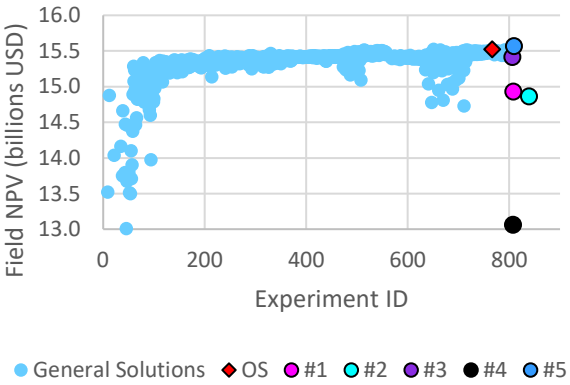

Source: created by the author.

Table 22 – Resulting NPV for OS and comparison cases, and NPV variation compared to the OS.

Solution	**NPV (billions USD)**	**Variation of NPV in relation to OS (millions USD)**
OS	15.52	-
#1	14.93	- 593.6
#2	14.87	- 657.2
#3	15.42	- 105.4
#4	13.06	- 2,459.4
#5	15.57	44.2

Source: Created by the author.

The optimal solution (OS) was found in experiment number 766, highlighting the greater difficulty of the process in relation to previous cases, where the optimal solution was obtained in the first experiments.

The optimal solution resulted in an NPV of 15.52 billion USD. The OS result was slightly below the idealized case #5, where there is no consideration of scaling effects in the perforations, with a difference of 44.2 million USD (a variation of 0.28%). This result highlights the importance of the treatment campaign, as an optimized execution can greatly reduce the value loss caused by the scaling effect in the perforations, almost eliminating it altogether.

The NPV values for the cases where there is no CO_2-WAG exchange, #1 and #2, were very close to each other, with values of 14.93 and 14.87 billion USD, respectively. These results were, on average, 4% lower than the NPV obtained for the OS, representing a decrease in value

of approximately 625 million USD. The average NPV of #1 and #2 was less than 90% of all the experiments created by CMOST during the optimization process that utilized the CO_2-WAG strategy, indicating the importance of using the CO_2-WAG.

Like the results of phase 1 of the research, the case that considers treatments always performed preventively, Case #3, did not yield the highest NPV, falling 105.4 million USD below the result found for the OS, indicating the importance of determining the optimal point for treatment execution. However, this difference represents a variation of only 0.68% in NPV compared to the optimal solution, indicating that the preventive treatment solution can be adopted as a simplified and high-quality strategy.

Among the comparison cases, case #4, where treatments were not allowed, resulted in the lowest NPV of 13.06 billion USD, representing a reduction of 2.459 billion USD (15.8%) compared to the OS. This result highlights the importance of conducting and optimizing the treatment campaign. The NPV reduction of case #4 compared to case #5 was 16%, indicating the risk of significant value loss for the field by not considering scaling effects and performing treatments.

Figure 28 presents the resulting time series for NPV (Figure 28a), number of treatments (Figure 28b), cumulative oil (Figure 28c), gas (Figure 28d), and water production (Figure 28e), as well as cumulative gas (Figure 28f) and water injections (Figure 28g), for the OS and the comparison cases. It can be observed from the Figure 28a that the OS consistently exhibits a significantly higher NPV compared to the solutions of cases #1, #2, and #4 throughout the entire simulated horizon, consistently slightly above case #3 and below the idealized case #5. These results indicate the consistency of adopting the OS strategy, even for different production horizons.

As it can be observed in Figure 28b, Among the cases where treatments are performed (OS, #1, #2, and #3), the number of treatments in the OS is always lower than those performed by the other solutions, resulting in lower treatment costs. This demonstrates the success of the computational effort in the optimization process.

In fluid production, the cumulative oil curve (Figure 28c) follows the same trend as the NPV, with the OS slightly lower than the idealized solution #5 and slightly higher than the preventive treatment solution #3. The cases without the CO_2-WAG strategy, #1 and #2, exhibit similar curves to each other, but significantly lower than the OS. The case #4, without any treatments, shows the lowest oil production curve. The significant decrease in production in this case occurs due to scale associated with the lack of treatments. As can be seen in Figure 29a, in case #4 all wells reach the minimum individual BHP to increase production. Despite

this, no well shuts down and the SPU maintains residual production until the end of the simulation horizon (Figure 29b).

Gas production (Figure 28d) showed similar trends for all cases, except for Case #4, where, like the oil curve, it starts to become lower than the others from year 8 of the simulated horizon.

The cumulative water production curves (Figure 28e) exhibit considerable dispersion, but consistent trends throughout the entire simulated period. Notably, there is a significant reduction in water production for the OS compared to cases #1, #2, and #3, and a slight reduction compared to case #5. This implies lower costs for treating the produced water in the OS. The water production for case #4 was lower than all other cases, consistent with the lower production of other fluids for this case.

Fluid injection (gas and water) showed similar trends for the OS, #1, #2, #3, and #5 cases. In case #4, there is lower gas injection (Figure 28f) due to lower production, as the produced gas is reinjected into the reservoir. The lower water injection (Figure 28g) for case #4 is also related to the lower fluid production, resulting in a reduced need for injection to reach the target pressure determined for the reservoir.

Figure 28 – Time series for NPV, number of treatments, cumulative productions, and fluid injections in the reservoir for the OS and comparison cases.

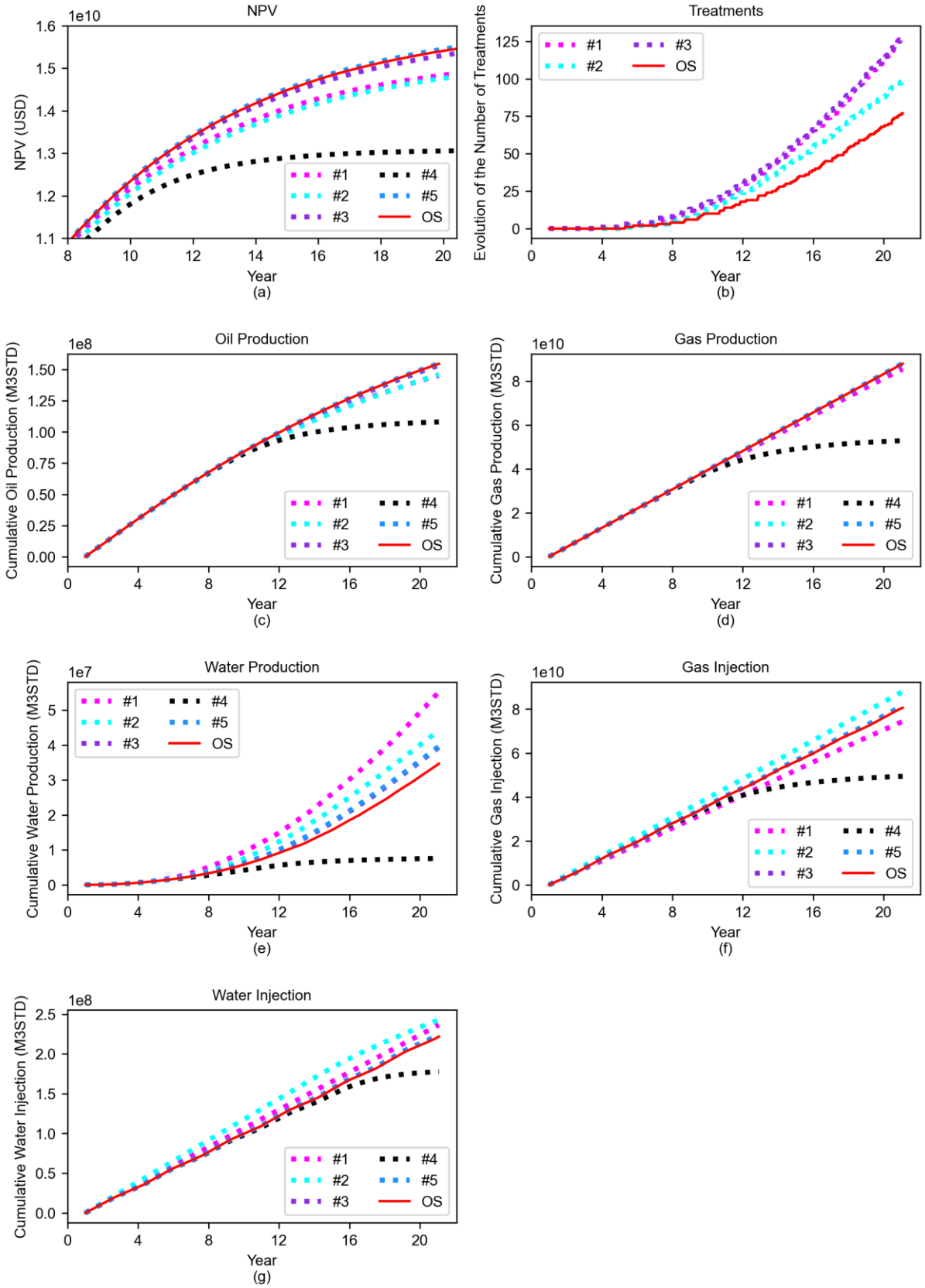

Source: created by the author.

Figure 29 – Time series of bottom hole pressure (BHP) for the wells in comparative Case #4 (a) and oil production rate curve for OS and comparative Case #4.

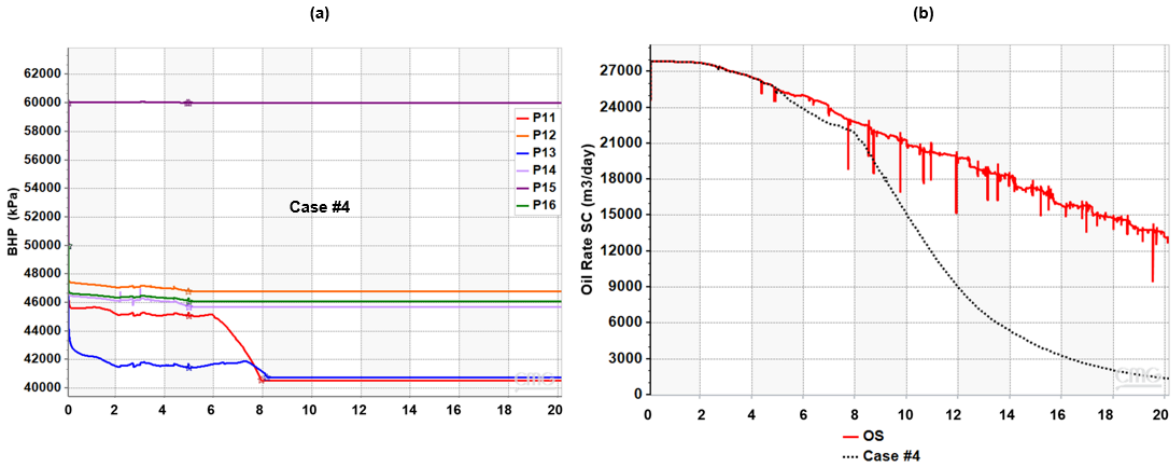

Source: created by the author.

The optimized parameters setup found for the OS, as well as the results for NPV and the total number of treatments and treatments per well, are presented in Table 23.

Overall, it is observed that the treatment target results behaved differently compared to the outcomes for the Cutout in the first phase of the research, where the specified targets for *J* reduction treatments (sr_i) decreased as the water cut (i-index) increased. However, the solutions found in Table 23 for the complete model (Case 4) indicate some variability in determining the sr_i. Only in the case of well P13, there was a consistent trend of decreasing sr_i with increasing water cut. This effect can be explained by the greater complexity involved in the joint production of six producer wells operating in the same SPU with limited capacities, where the reduction in oil production from one well can be compensated by adjusting the production of others (the first phase of the research involved only one producer well, and this production adjustment was not possible). Another factor that possibly influenced this behavior in determining the optimized sr_i was the dynamics of flow in porous media, where there are mutual interactions between the effects caused by the joint production and injection of multiple wells. This result indicates that the correct approach is the joint evaluation of the wells in the complete model, as performed in Case 4, rather than individual well assessments. Well P13 also received the lowest number of treatments, only 6. This result was most likely influenced primarily by the relatively low water cut curve of the well compared to the others (Figure 31).

The optimal target for reservoir pressure (P_m) in the complete model was found to be 68,400 kPa, significantly higher than the value found for the Cutout model of 59,400 kPa. Despite this high target value for P_m, the maximum average pressure reached by the reservoir

was 63,608 kPa, at the end of the production horizon (Figure 30a). This pressure is also higher than the initial reservoir pressure of 62,000 kPa. The relatively high value of P_m found in the OS must be related to the effect of decreasing scaling tendency at higher pressures.

The optimal duration for the CO_2-WAG cycles (SWC) was determined to be 1,206 days, which is also significantly higher than the scaled Cutout model where SWC resulted in 244 days. Once again, these results emphasize the importance of considering the complete model in the analysis.

As the result of the OS, 77 treatments are performed throughout the simulation horizon, with a final NPV, as mentioned before, of 15.52 billion USD.

Table 23 – Optimized parameters found for Case 4 (OS) and results for NPV and number of treatments performed.

Parameter	Field	Producer Wells					
		P11	**P12**	**P13**	**P14**	**P15**	**P16**
Optimized setup of decision parameters							
sr1	--	61.6%	25.3%	98.0%	9.1%	69.7%	57.6%
sr2	--	96.0%	82.8%	67.7%	40.4%	51.5%	96.0%
sr3	--	96.0%	82.8%	67.7%	9.1%	78.3%	59.6%
sr4	--	96.0%	82.8%	67.7%	9.1%	78.3%	59.6%
BHP (kPa)	--	40,548	46,800	40,746	45,709	60,000	46,106
Pm (kPa)	68,400	--	--	--	--	--	--
SWC (days)	1,206	--	--	--	--	--	--
Results							
Total Treatments	77	16	14	6	10	14	17
NPV (billions USD)	15.52						

Source: Created by the author.

Figure 30 presents a graph showing the evolution of the WAG Ratio (water injected volume divided by gas injected volume under reservoir conditions) and a graph showing the evolution of injected water and gas volumes (under surface conditions) over the WAG cycles. It can be observed that the 1206-day SWC resulted in 6 complete cycles of CO_2-WAG exchanges, plus one incomplete cycle. The WAG Ratio results for Cluster A start at a slightly higher value than 1 for the first cycle and evolve to an approximate value of 1.1 in the sixth cycle, indicating a gradual increase in water injection. This increase is consistent with the increase in water production caused by the influx of injected water into the producers, resulting in an increase in water cut, which in turn leads to a greater tendency for reservoir depressurization (decrease in mass balance between injected and produced fluids), increasing

the need for water injection. The graph also shows that the reservoir pressure in the first cycle, approximately 62,200 kPa, is 2600 kPa away from the target pressure of 64,800 kPa (Pm), requiring a positive mass balance in the reservoir to reach Pm. For Cluster B, the WAG Ratio remained consistently around 1 throughout all 6 complete cycles, which occurred due to injection reaching the operational limit in the wells of this cluster, which has only 3 wells (Cluster A has 4 wells). In the graph showing the evolution of injected water and gas volumes in Figure 30, an increase in injected water volumes can be observed throughout the cycles, in line with the effects observed in the WAG Ratio graph. Gas injection remained constant throughout all cycles, conditioned by the production of this fluid and the operational limits imposed by SPU capacity.

In addition to the graphs related to the CO_2-WAG cycles, Figure 30 also presents a graph with the time series resulting from the Optimal Solution (OS) for the treatments performed in the field, a graph with the evolution of the average daily oil and liquid flow rate, a graph for the average daily water and gas production rate, and a graph with the evolution of the water cut (%) and Gas-Oil Ratio (GOR) over the 20-year production.

It can be observed that the number of treatments follows an exponential increasing trend, with approximately 15 treatments performed in the first 12 years of the horizon and 65 treatments performed in the following eight years, which was expected as the scale is inherently related to water production, which continuously increases over the horizon.

The oil production declines over the years, primarily due to the increase in water production, but also due to the increase in Gas-Oil Ratio (GOR). The SPU is capped at a gas production of 12 million m^3 STD throughout the entire horizon, so the increase in GOR leads to a decrease in oil production and, consequently, also reduces the total production of liquids (water plus oil).

Figure 30 – CO_2-WAG and optimal solution (OS) analysis, production trends, and treatment evolution for field.

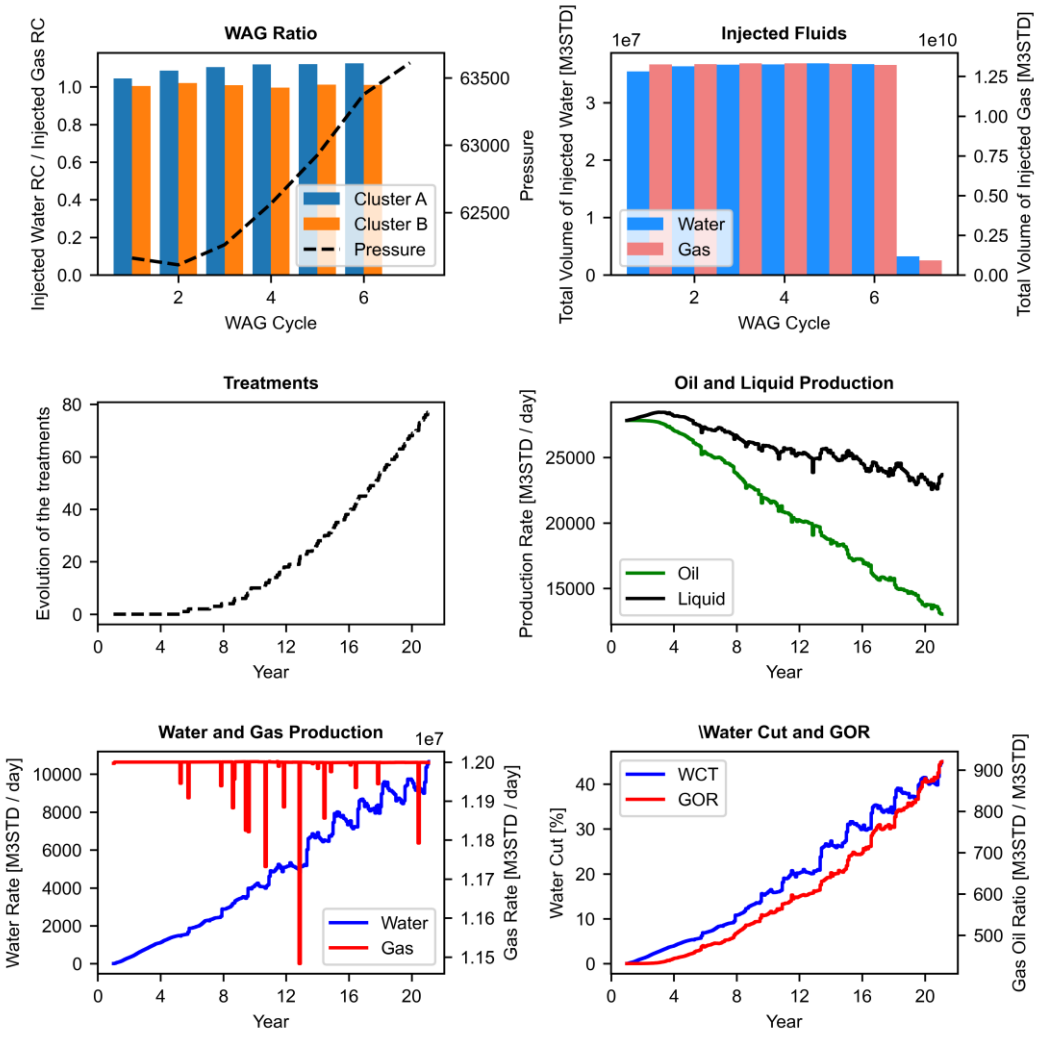

Source: created by the author.

The production curves for each producing well (average daily oil rate, water cut (%), and GOR) and the time series of treatments and cumulative water production are shown in the graphs of Figure 31.

It is observed that, as mentioned earlier, the decision regarding the best setup for treatment design is not evident due to the trade-off of multiple operational variables related to production and injection from multiple wells for the same SPU. The analysis of Figure 31 shows that well P14, despite having the highest cumulative water production, has only undergone 10 treatments, while wells P11, P12, P15, and P16, which have lower cumulative water production, have undergone a total of 16, 14, 14, and 17 treatments, respectively. This deprioritization of

well P17 occurs because it has the highest tendency for increasing GOR, where the SPU remains gas-limited throughout the production horizon, as can be observed from Figure 30. The well that received the fewest treatments was P13, which, despite its relatively low GOR curve, has a significantly lower water production curve than the other wells, requiring fewer treatments.

Figure 31 – Production curves and treatment time series (by well).

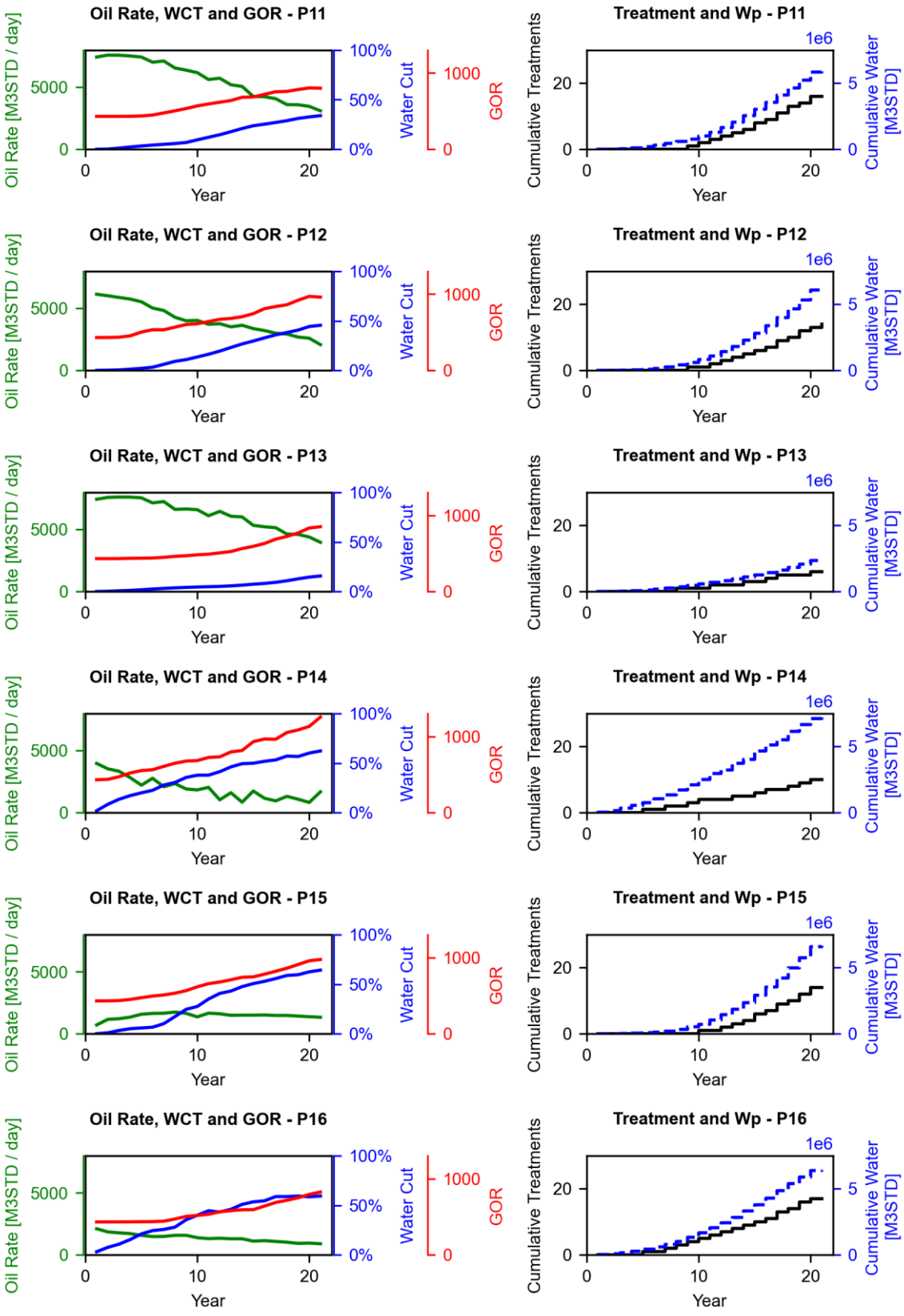

Source: created by the author.

6. CONCLUSIONS

This study presents an innovative methodology for calculating scale effects in both reservoirs and wellbore perforations. The methodology combines a flow simulation with reactive transport (FSRT) model for the reservoir dimension and an analytical model for the wellbore perforations dimension. By integrating the analytical model into the FSRT, the methodology enables the calculation of precipitated scale mass in the wellbore perforations and its impact on well productivity reduction during simulation time.

In the first phase, a simplified proxy was created to calculate the precipitable mass, and the optimization process was divided into two optimization stages (CO2-WAG stage and treatments stage). Three case studies were conducted, with Case 1 focusing on CO_2-WAG optimization alone (first stage), and Cases 2 and 3 considering scale treatments performed by rig or remotely by the SPU (second optimization stage).

Conclusions from the first phase:

- Optimization of CO_2-WAG parameters resulted in a gain of 11% to 15% in NPV compared to cases that did not utilize the method.
- The solution that did not account for the scale effect in wellbore perforations was overestimated by 8.4% compared to the case of remote treatment and 10.7% compared to treatments performed by rig.
- Remote operations had a 2.1% higher NPV (11.7 million USD) than those performed by rig, with 2 additional treatments.
- Treatments become less attractive as water production increases.
- The strategy of preventive treatments did not yield the highest NPV.
- The implementation of treatments resulted in a gain of 44 to 55 million USD, respectively for cases with rig treatments and remote treatments.

The second phase involved refining the proxy for the chemical equilibrium simulator and conducting the optimization process in a single stage. An analytical expression was developed through linear regression to accurately calculate the precipitable mass based on ionic concentrations. This improved methodology was applied to the full UNISIM-III model in Case 4, which included multiple wells and a longer production horizon.

Conclusions from the second phase:

- Refinement of the proxy for the chemical equilibrium simulator and conducting the optimization process in a single stage resulted in an optimal NPV.

- The optimal solution had an NPV that was 0.28% lower than the idealized case without scale, demonstrating that the optimized treatment can mitigate a significant portion of the losses.
- The cases that did not utilize CO_2-WAG had an average NPV that was 4% lower (625 million USD).
- Similar to Phase 1, the strategy of always performing preventive treatments resulted in an NPV lower than the optimal solution, with a 0.68% difference.
- The results indicate a significant gain from the treatment campaign, with the optimized solution being 2.5 billion USD (15.8%) higher than the case where treatments are not performed.

6.1 Overall conclusion:

The developed methodology proved to be effective in optimizing CO_2-WAG injections and scale treatments in well perforations. It provides valuable insights for decision-making in reservoir management, resulting in improved NPVs and reduced treatment costs. The findings underscore the importance of considering scale effects and implementing optimized treatment strategies to maximize the economic value of oil production in fields subject to scale occurrence.

6.2 Final considerations.

The methodology presented in this work can be used in several field studies that involve the need to model the scale and the prediction of its effects on production. Some of the potential applications for the method presented in this work are:

e) Production optimization studies;
f) Analysis of well uncertainties under scale effect;
g) Evaluation of alternative treatment scenarios;
h) Treatment campaign planning;
i) Adjustment of production history of wells subject to scale.

6.3 Future work

In future work, the predictive capacity of the developed method is intended to be evaluated by applying it to real historical production data from wells that have experienced scale effects and have undergone acid cleaning and inhibition treatments. Additionally, other

studies may assess the uncertainty associated with economic variables, such as oil prices, or scale parameters, such as deposition composition, mineral composition of the porous medium near the producer, deposition radius around the well, and uncertainty in the ionic compositions produced and the precipitable mass. Future studies with the proposed method could also evaluate possible injectivity loss caused by the interaction of the injected water with the formation water, especially in reservoirs that do not use CO_2-WAG.

REFERENCES

ADEGBITE, J. O.; AL-SHALABI, E. W.; GOSH, B. Modeling the effect of engineered water injection on oil recovery from carbonate cores. **SPE International Conference on Oilfield Chemistry**, Montgomey, Texas, USA. SPE 184505, 2017.

ALLISON, J.D.; BROWN, D.S.; NOVO-GRADAC, K.J. **MINTEQA2/PRODEFA2, A geochemical assessment model for environmental systems version 3.0 user's manual.** Environmental Research Laboratory, Office of Research and Development, U.S. Environmental Protection Agency, Athens, Georgia, p.106, 1990.

ARAÚJO, C. H. V. **Simulação do Transporte Reativo durante a injeção de água e CO2 em Reservatórios Carbonáticos**. Dissertação (Mestrado em Tecnologia de Processos Químicos e Bioquímicos) – Universidade Federal do Rio de Janeiro, Escola de Química, Rio de Janeiro, 2012.

ARAÚJO, T. P.; LEITE, M. G. P. Flow simulation with reactive transport applied to carbonate rock diagenesis. **Marine and Petroleum Geology**, v. 88, p. 94-106, 2017.

AZARI, V.; RODRIGUES, H.; SUIESHOVA, A.; VAZQUEZ, O.; MACKAY, E. Long-term Strategy Optimization of Scale Squeeze Treatment in a Carbonate Reservoir Under CO_2-WAG Water-Alternating-Gas Injection. **SPE International Conference on Oilfield Chemistry**, The Woodlands, Texas, U.S., Nov. 2021. SPE-204352-MS.

BADER, M. S. H. Sulfate removal technologies for oil fields seawater injection operations. **Journal of Petroleum Science and Engineering**, v. 55, n. 1-2, p. 93-110, 2007.

BEDRIKOVETSKY, P.; SILVA, R.M.P; DAHER, J.S.; GOMES, J.A.T.; AMORIM, V.C. Well-data-based prediction of productivity decline due to sulphate scaling. **Journal of Petroleum Science and Engineering,** n. 68, p. 60-70. 2009.

CHARLTON, S. R.; MACKLIN, C.L.; PARKHURST, D. L. PHREEQC - a graphical user interface for the geochemical computer program PHREEQC. **Water-Resources Investigations Report**, v.9, p. 7-4222. U.S. Geological Survey, Lakewood, CO, USA. 1997.

CHAUHAN, K.; SHARMA, P.; CHAUHAN, G. S. Removal/dissolution of mineral scale deposits. In: **Mineral scales and deposits**, Elsevier, 2015. chap. 29, p. 701-720.

COMPUTER MODELLING GROUP. **BUILDER User's Guide**, Calgary 2019.

COMPUTER MODELLING GROUP. **CMOST AI User Guide**, Calgary 2019.

COMPUTER MODELLING GROUP. **GEM Technical Manual**, Calgary 2019.

COMPUTER MODELLING GROUP. **WINPROP User Guide**, Calgary 2019.

CORREIA M., HOHENDORFF J., GASPAR A.T.F.S., SCHIOZER D. UNISIM-II-D: Benchmark Case Proposal Based on a Carbonate Reservoir. **SPE Latin American and Caribbean Petroleum. Engineering Conference,** Quito, Ecuador 1, p.18–20, 2015.

CORREIA, M.; BOTECHIA, V.; PIRES, L.; RIOS, V.; SANTOS, S.; HOHENDORFF, J.; CHAVES, M.; SCHIOZER, D. UNISIM-III: Benchmark Case Proposal Based on a Fractured Karst Reservoir. **ECMOR XVII – 17th European Conference on the Mathematics of Oil Recovery**, Online Event, 14-17, 2020.

ENERGY INFORMATION ADMINISTRATION (EIA). **Annual Energy Outlook**, 2023. Available online: https://www.eia.gov. Accessed on October 2023.

ENERGY INFORMATION ADMINISTRATION (EIA). **Europe Brent Spot Price FOB (Dollars per Barrel)**, 2024. Available online: https://www.eia.gov/dnav/pet/hist/LeafHandler.ashx?n=PET&s=RBRTE&f=M. Accessed on April 2024.

FONSECA, T.U. **Acidificação: fluidos de perfuração e hidráulica de poço**. Petrobras Training Program, Salvador, BA, Brazil, 2010.

GOMES FILHO, L. C.; SAMPAIO, M. A.. Well Production Optimization under the Scale Effect and CO2-WAG Injection in a Carbonate Model of the Brazilian Pre-Salt. **SPE Production & Operations**, v. 38, n. 01, p. 35-50, 2023.

HAJIREZAIE, S.; WU, X.; SOLTANIAN, M, R,; SAKHA, S. Numerical simulation of mineral precipitation in hydrocarbon reservoirs and wellbores. **Fuel Journal**, [s.l.], 238, p. 462–472, 2019.

HARVEY, A.H. Semiempirical correlation for Henry's constants over large temperature ranges. **AIChE journal**, v. 42, n.5, p. 1491-1494, 1996.

IHS Markit. **Petrodata Offshore Rig Day Rate Trends**, 2022. Available online: https://ihsmarkit.com/products/oil-gas-drilling-rigs-offshore-day-rates.html.

KAASA, B, **MultiScale manual**, Exprogroup, 2009.

KAMALA, M. S.; HUSSINB, I.; MAHMOUDC, M., SULTANC, A. S.; SAADD, M. A. S.; Oilfield Scale formation and chemical removal: A review**. Journal of Petroleum Science and Engineering**. 171, p. 127–139, 2018.

KANG, W.; WANG, T.; ZHANG H.; HOU, X.; YANG H. A dynamic scale location monitor method to predict oilfield blockage during water flooding. **Journal of Petroleum Science and Engineering**. V 191. Article 107168. 2020.

LEAL, A. M. M. Reaktoro: **An open-source unified framework for modeling chemically reactive systems**, 2015. Available online: https://reaktoro.org.

LI, Y.-K.; NGHIEM, L.X. Phase equilibria of oil, gas and water/brine mixtures from a cubic equation of state and Henry's law. **The Canadian Journal of Chemical Engineering**, v. 64, n. 3, p. 486-496, 1986.

MACKAY, E. J.; JORDAN, M. M.; FEASEY, N. D.; SHAH, D; KUMAR, P; ALI, S. A.. Integrated risk analysis for scale management in deepwater developments. **SPE Production & Facilities**, v. 20, n. 02, p. 138-154, 2005.

MIRANDA, D. E. O. **Impacto do preço de robustez na definição da estratégia de produção de petróleo.** Dissertação (Mestrado) - Faculdade de Engenharia Mecânica e Instituto de Geociências, Universidade Estadual de Campinas, Campinas, São Paulo, 2018.

NOVAES, A. M. **Recuperação secundária de petróleo com injeção de água do mar:** efeitos da interação rocha-fluido. Dissertação (Mestrado) - Escola de Química, Universidade Federal do Rio de Janeiro, Rio de Janeiro, 2016.

PETROBRAS. **Teste de Longa Duração e Sistemas de Produção Antecipada de Libra – Bacia de Santos – II**. Caracterização da Atividade. In Portuguese. Available in: http://licenciamento. ibama. gov. br/Petroleo/Producao/Producao, 2015.

REGINATO, L. F.; PEDRONI, L. G.; COMPAN, A. L. M.; SKINNER, R.; SAMPAIO, M. A. Optimization of ionic concentrations in engineered water injection in carbonate reservoir through ANN and FGA. **Oil & Gas Science and Technology – Rev. IFP Energies Nouvelles**, v. 76, p. 13, 2021.

RODRIGUES, H.; MACKAY, E.; ARNOLD, D.; SILVA, D. Optimization of CO_2-WAG and Calcite Scale Management in Pre-Salt Carbonate Reservoirs. **Offshore Technology Conference**, Rio de Janeiro, BR. OTC-29823-MS, 2019.

RODRIGUES, H.; MACKAY, E.; ARNOLD, D.; AZARI, V.; VAZQUEZ, O. Economic optimization and calcite scale management of CO_2-EOR in carbonate reservoirs. **SPE International Oilfield Scale Conference and Exhibition**, virtual event. SPE-200678-MS, 2020.

RODRIGUES, V. F.; NEUMANN, L. F.; MIURA, K; TINOCO, F. L.; NETTO, J. B. M. L.; DAHER, J. S. Formation Damage history in the mature fields of Campos Basin Offshore Brazil. **SPE European Formation Damage Conference and Exhibition**. Scheveningen, The Netherlands. SPE 106389-MS, 2007.

ROSA, A. J.; DE SOUZA CARVALHO, R.; XAVIER, J. A. D. **Engenharia de reservatórios de petróleo**. Interciência, Rio de Janeiro, RJ, BR, 2006.

SAMPAIO, M. A.; DE MELLO, S. F.; SCHIOZER, D. J. Impact of physical phenomena and cyclical reinjection in miscible CO_2-WAG recovery in carbonate reservoirs. **Journal of Petroleum Exploration and Production Technology,** v. 10, p. 3865–3881, 2020.

SHABANI, A.; KALANTARIASL, A.; PARVAZDAVANI, M; ABBASI, S. A reactive transport approach for modeling Scale formation and deposition in water injection wells. **Journal of Petroleum Science and Engineering**, v. 190, p. 107031, 2020.

STAMATAKIS, E.; STUBOS, A.; MULLER J. Scale prediction in liquid flow through porous media: A geochemical model for the simulation of $CaCO_3$ deposition at the near-well region. **Journal of Geochemical Exploration**, v. 108, n2, p. 115-125, 2011.

YUAN, B.; WOOD, D. A. A comprehensive review of formation damage during enhanced oil recovery. **Journal of Petroleum Science and Engineering**, v. 167, p. 287-299, 2018.